

# *Abrupt stratospheric vortex weakening associated with North Atlantic anticyclonic wave breaking*

Article

Accepted Version

Lee, S. H., Charlton-Perez, A., Furtado, J. C. and Woolnough, S. (2019) Abrupt stratospheric vortex weakening associated with North Atlantic anticyclonic wave breaking. *Journal of Geophysical Research: Atmospheres*, 124 (15). pp. 8563-8575. ISSN 2169-897X doi:  
<https://doi.org/10.1029/2019JD030940> Available at  
<https://centaur.reading.ac.uk/85477/>

It is advisable to refer to the publisher's version if you intend to cite from the work. See [Guidance on citing](#).

Published version at: <http://dx.doi.org/10.1029/2019JD030940>

To link to this article DOI: <http://dx.doi.org/10.1029/2019JD030940>

Publisher: American Geophysical Union

All outputs in CentAUR are protected by Intellectual Property Rights law, including copyright law. Copyright and IPR is retained by the creators or other copyright holders. Terms and conditions for use of this material are defined in the [End User Agreement](#).

[www.reading.ac.uk/centaur](http://www.reading.ac.uk/centaur)

**CentAUR**

Central Archive at the University of Reading

Reading's research outputs online

# Abrupt stratospheric vortex weakening associated with North Atlantic anticyclonic wave breaking

S. H. Lee<sup>1</sup>, A. J. Charlton-Perez<sup>1</sup>, J. C. Furtado<sup>2</sup>, and S. J. Woolnough<sup>3,1</sup>

<sup>1</sup>Department of Meteorology, University of Reading

<sup>2</sup>School of Meteorology, University of Oklahoma

<sup>3</sup>National Centre for Atmospheric Science, University of Reading

## Key Points:

- In early February 2018, forecasts abruptly transitioned from indicating a strong stratospheric polar vortex to sudden stratospheric warming.
- This was due to the predictability of a cyclone in the North Atlantic which was associated with driving an anticyclonic Rossby wave break.
- Similar historical cases show this as a mechanism for weakening the stratospheric polar vortex which can lead to major sudden warmings.

**Abstract**

The sudden stratospheric warming (SSW) of 12 February 2018 was not forecast by any extended-range model beyond 12 days. From early February, all forecast models that comprise the subseasonal-to-seasonal (S2S) database abruptly transitioned from indicating a strong stratospheric polar vortex (SPV) to a high likelihood of a major SSW. We demonstrate that this forecast evolution was associated with the track and intensity of a cyclone in the north-east Atlantic, with an associated anticyclonic Rossby wave break, which was not well-forecast. The wave break played a pivotal role in building the Ural high, which existing literature has shown was a precursor of the 2018 SSW. The track of the cyclone built an anomalously strong sea-level pressure dipole between Scandinavia and Greenland (termed the S-G dipole) which we use as a diagnostic of the wave break. Forecasts which did not capture the magnitude of this event had the largest errors in the SPV strength and did not show enhanced vertical wave activity. A composite of 49 similarly strong wintertime (November–March) S-G dipoles in reanalysis shows associated anticyclonic wave breaking leading to significantly enhanced vertical wave activity and a weakened SPV in the following days, which occurred in 35% of the 15-day periods preceding observed major SSWs. Our results indicate a particular transient trigger for weakening the SPV, complementing existing results on the importance of tropospheric blocking for disruptions to the Northern Hemisphere extratropical stratospheric circulation.

**Plain Language Summary**

During winter, a large circulation 10-50 km above the pole (known as the stratospheric polar vortex) can influence the day-to-day weather patterns in the troposphere beneath from weeks to months later. Thus, being able to predict the behavior of the stratospheric polar vortex is important for predicting the weather on longer time-frames. In February 2018, the Northern Hemisphere stratospheric polar vortex broke apart in an event known as a sudden stratospheric warming, which was not well-forecast. This event led to unusually cold conditions across Eurasia. In this article we find the poor predictability of the event was due to a poorly forecast weather system in the Atlantic. We also show that this pattern was present in previously observed cases where the stratospheric polar vortex has weakened. Our results demonstrate a trigger mechanism for these extreme events and have implications for our ability to predict the weather at longer ranges.



## 1 Introduction

The major mid-winter sudden stratospheric warming (SSW) event of 12 February 2018 was the first major SSW since January 2013 (defined as a reversal of the daily-mean 10 hPa 60°N zonal-mean zonal winds (Charlton & Polvani, 2007)), a 5 year gap which was the longest since 1989–1998 according to the SSW Compendium (Butler, Sjoberg, Seidel, & Rosenlof, 2017). It produced a split of the stratospheric polar vortex (SPV) into two smaller vortices. Following the metric of Karpechko, Hitchcock, Peters, and Schneider (2017) the event was downward-propagating with the negative phase of the stratospheric Northern Annular Mode (NAM) (Baldwin & Dunkerton, 2001; Thompson & Wallace, 2000) accompanied by a strong and persistent negative tropospheric NAM in the 45 days following the event. The negative tropospheric NAM and associated negative North Atlantic Oscillation (NAO) produced extremely cold conditions across Europe and northern Asia, with a large anticyclone over Scandinavia generating a cold easterly flow (Ferranti, Magnusson, Vitart, & Richardson, 2018). With such a high impact response, the ability to predict the onset of an SSW like in 2018 is of vital importance for sub-seasonal forecasting.

The 2018 SSW was the first to occur following the development of the subseasonal-to-seasonal (S2S) database of extended-range forecasts from 11 international forecast models (Vitart et al., 2017). None of the S2S model forecasts issued at the time indicated a major SSW until early February (Karpechko, Charlton-Perez, Balmaseda, & Vitart, 2018), giving a predictability window less than the medium-range timeframe ( $\sim 2$  weeks). Although this lies within the window typical of predicting major SSWs (Taguchi, 2014; Tripathi et al., 2016, 2015), S2S model forecasts abruptly transitioned from projecting a strong SPV to a weak SPV/major SSW in late January-early February, with a corresponding transition in forecasts of tropospheric conditions (such as from forecasts of a positive NAO to a negative NAO). Karpechko (2018) showed several SSWs were poorly forecast in ECMWF hindcasts at lead-times beyond 7–10 days, but most were generally associated with a longer-range signal of SSW likelihood.

Specifically for the February 2018 event, Karpechko et al. (2018) examined S2S model forecasts from 1 February onwards and showed a strong relationship between the accuracy of stratospheric wind forecasts and the intensity of an anticyclone over the Urals (named the ‘Ural high’). However, they did not assess the longer-term predictability of

77 the event, the mechanism driving the onset of the Ural high, or its influence on the strato-  
78 sphere, leaving open questions about the abrupt predictability onset. The Ural high has  
79 also been shown to drive SPV variability (Peings, 2019; White et al., 2019) by project-  
80 ing onto the climatological stationary wave pattern.

81 Most studies of SSW precursors use a ‘top-down’ perspective, where the tropospheric  
82 features are analyzed in the period preceding observed stratospheric events. These ap-  
83 proaches typically discern stationary or longer-lived features through the process of av-  
84 eraging anomalies in the build-up to SSWs. Tropospheric blocking is one such feature  
85 (e.g. Colucci & Kelleher, 2015; Garfinkel, Hartmann, & Sassi, 2010; Julian & Labitzke,  
86 1965; Martius, Polvani, & Davies, 2009; Quiroz, 1986). For example, Bao, Tan, Hart-  
87 mann, and Ceppi (2017) used cluster analysis to assess 500 hPa geopotential height pat-  
88 terns in the month before 37 SSWs in reanalysis, and found the patterns to be associ-  
89 ated with linear interference with climatological stationary waves. Kolstad and Charlton-  
90 Perez (2011) used reanalysis alongside climate model simulations and found a particu-  
91 larly strong signal for a height anomaly dipole over northern Eurasia preceding ‘weak  
92 vortex months’. Other studies have considered more transient features associated with  
93 specific stratospheric events. Coy, Eckermann, and Hoppel (2009) noted the importance  
94 of zonal wavenumbers 4-5 associated with synoptic-scale systems preceding the SSWs  
95 of January 2006 and 2003. They implicated tropospheric systems over the North Atlantic  
96 and subtropical wave breaking; forecasting experiments showed a realistic SSW only oc-  
97 curred when a North Atlantic weather system was correctly represented in the model.  
98 On the other hand, a study of the January 2013 SSW (Coy & Pawson, 2014) suggested  
99 a rapidly-deepening cyclone in the North Atlantic played only a minor role, acting as a  
100 transient source of vertical wave activity that was not crucial to forcing the event. The  
101 authors also remark on the dynamical link between the initial stratospheric vortex state  
102 and the track of the cyclone, suggesting a two-way relationship. O’Neill, Oatley, Charlton-  
103 Perez, Mitchell, and Jung (2017) demonstrated a link between extratropical tropospheric  
104 cyclogenesis occurring at the edge of the SPV and split-type SSWs through a potential  
105 vorticity framework. Although mainly focusing on the Southern Hemisphere SSW of 2002  
106 (e.g. Krüger, Naujokat, & Labitzke, 2005), they briefly show a similar mechanism with  
107 cyclogenesis over the eastern seaboard of the Northern Hemisphere continents. Most  
108 recently, Attard and Lang (2019) approach the problem by looking at the meridional eddy  
109 heat flux, and demonstrate the different responses for blocks and ‘bomb’ cyclones in the

110 Atlantic and Pacific sectors. They conclude cold-season Atlantic bomb cyclones and Pa-  
 111 cific blocks were associated with negative heat flux anomalies (and vice versa) whilst also  
 112 noting that only a relatively small number of blocks and bombs are actively associated  
 113 with SSWs.

114 Thus, there exist both transient and stationary drivers of stratospheric variabil-  
 115 ity (including but not limited to SSWs), the predictability of which plays a role in the  
 116 onset of SSW prediction. In this study, we provide a dynamical explanation for the abrupt  
 117 transition in the forecasts of the February 2018 event, building upon existing analysis.  
 118 We demonstrate that this is a characteristic of historical cases of vortex weakening, rather  
 119 than unique to the flow configuration driving the 2018 event, through a ‘bottom-up’ ap-  
 120 proach (analysing the response of the stratosphere to tropospheric events). Our results  
 121 have implications for extended-range predictability of SSWs and thus sub-seasonal tro-  
 122 pospheric forecasts.

## 123 **2 Data and Methods**

124 We use forecast data from the European Centre for Medium Range Weather Fore-  
 125 casts (ECMWF) and National Centers for Environmental Prediction (NCEP) models,  
 126 as these provide a combination of both large ensemble sizes and frequent launch dates  
 127 - ECMWF launches twice weekly (Tuesday and Thursday) with 51 members, and NCEP  
 128 launches daily with 16 members. The predictability onset of the SSW was common across  
 129 all the S2S models (Karpechko et al., 2018), so our analysis is not sensitive to the choice  
 130 of model. For verification, we use the ECMWF ERA-Interim reanalysis (Dee et al., 2011).  
 131 The strength of the SPV is defined using the zonal-mean zonal wind at 10 hPa and 60°N  
 132 ( $U_{10_{60}}$ ). We use 45–75°N meridionally-averaged zonal-mean eddy heat flux (denoted as  
 133  $[v^*T^*]$  where the star notation indicates a departure from the zonal-mean, and square  
 134 brackets indicate a zonally-averaged quantity) at 300 hPa as a proxy for upper-tropospheric  
 135 wave activity. This is proportional to the vertical component of the Eliassen-Palm flux  
 136 (Andrews, Holton, & Leovy, 1987). Standardized polar cap (60–90°N) geopotential height  
 137 anomalies are used as a proxy for the NAM index (Karpechko et al., 2017); the anoma-  
 138 lies are inversely proportional to the index. Unless otherwise stated, standardized anoma-  
 139 lies are computed with respect to the climatological daily-mean and standard deviation  
 140 in ERA-Interim. Historical composites use data from January 1979–March 2017 inclu-  
 141 sive, and statistical significance is assessed using a bootstrap re-sampling method with

142 replacement ( $n = 50,000$ ) for November–March in the period January 1979 to March 2017.  
 143 Potential vorticity is analyzed on the 315 K isentropic surface in ERA-Interim data and  
 144 the 320 K isentropic surface in model forecast data as these are the nearest tropospheric  
 145 levels available in both datasets. All data are re-gridded to  $2.5^\circ$  horizontal resolution for  
 146 consistency.

## 147 **3 Results**

### 148 **3.1 Characterizing the Onset of SSW Predictability**

149 To demonstrate the evolution of forecasts of the zonal-mean state, Figure 1 (a, c)  
 150 shows forecasts of  $U10_{60}$  for the first 5 days of the verifying SSW (12–16 February) for  
 151 all forecasts in which those dates featured. There is an abrupt transition in late January–  
 152 early February from forecasts of a strong vortex to a weakened vortex or major SSW.  
 153 In both ECMWF and NCEP systems, the 29 January ensembles showed no members in-  
 154 dicated mean easterlies during this period, with a tightly clustered ensemble. The fol-  
 155 lowing day, forecasts from NCEP substantially changed, with some members suggest-  
 156 ing a mean zonal wind reversal and the entire ensemble forecasting weaker  $U10_{60}$  than  
 157 the 25<sup>th</sup> percentile of the ensemble from the previous day – a change which also occurred  
 158 in the 29 January and 1 February ECMWF ensembles. There is also an increase in spread  
 159 despite the reduced lead-time. Ensemble spread was then much reduced by 5–6 Febru-  
 160 ary, a lead-time of only 6–7 days before the major SSW. A similar predictability evolu-  
 161 tion is found in other S2S models (not shown), indicating this was not related to the abil-  
 162 ity of certain models to capture the event. Moreover, we see the abrupt transition of vor-  
 163 tex strength was associated with an abrupt increase in 300 hPa [ $v^*T^*$ ] preceding the wind  
 164 reversal (Figure 1b and 1d). The increase in forecast heat flux suggests the low predictabil-  
 165 ity of the SSW was dependent on poorly-forecast tropospheric wave-driving, rather than  
 166 the response of the stratospheric vortex to a wave pulse or the sensitivity of the  $U10_{60}$   
 167 metric.

168 To investigate this evolution further, we look at the 29 January and 1 February en-  
 169 sembles from ECMWF, which cover the spread of evolutions from strong vortex to weak  
 170 vortex (Figure 2). The ensembles systematically diverge after 5 February – with the fore-  
 171 casts from 29 January showing low wave activity and strengthening zonal-mean zonal  
 172 winds, whilst the opposite is true for forecasts from 1 February. This is an even greater

173 divergence in zonal wind intensity than day-15 forecasts for the January 2013 SSW shown  
 174 in Tripathi et al. (2016). Despite the 3 day difference in lead-time, the systematic dif-  
 175 ference between the two ensembles motivates considering them together to capture the  
 176 uncertainty. Analysis in the corresponding NCEP ensembles gives similar results (see Fig-  
 177 ure S1).

178 Thus, there are two alternative scenarios demonstrated in ensemble forecasts from  
 179 late January and early February: (a) enhanced vertical wave activity around 5 Febru-  
 180 ary leading to SPV weakening, and (b) suppressed wave activity with little subsequent  
 181 change in SPV strength. In the next section, we discern the tropospheric drivers for these  
 182 divergent stratospheric evolutions.

### 183 **3.2 Characterizing Tropospheric Uncertainty**

184 Figure 3 depicts the linear correlation between the mean  $U10_{60}$  forecast for 9–11  
 185 February (a period where ensemble members either projected a quiescent vortex or strong  
 186 deceleration, c.f. Figure 2) and the mean sea-level pressure (MSLP) for 3–5 February (i.e.,  
 187 just before the onset of enhanced vertical wave flux). This correlation is calculated in  
 188 joined ensembles from 29 January to 1 February in NCEP (to increase ensemble sam-  
 189 ple size and incorporate a larger range of SPV strengths), and 29 January and 1 Febru-  
 190 ary in ECMWF; independent calculations (not shown) for the separate ensembles sug-  
 191 gest this is not a result of the difference in character of the forecasts or a facet of the dif-  
 192 ferences in lead-time. We average across forecasts initialized during the onset of predictabil-  
 193 ity of the vortex weakening event (c.f. Figure 1) to determine what changed during this  
 194 window. The results show the strongest correlations between the preceding MSLP field  
 195 and the strength of the SPV form a dipole between Scandinavia and Greenland. Secondary  
 196 regions of strong correlation are also located upstream and downstream of the main dipole.  
 197 The correlation field indicates that ensemble members with lower MSLP over eastern Green-  
 198 land and higher MSLP over Scandinavia forecast weaker  $U10_{60}$ . Based on this correla-  
 199 tion analysis, we define the Scandinavia-Greenland dipole in MSLP (hereafter, the S-G  
 200 dipole) to describe the evolution. We calculate this by subtracting the area-average MSLP  
 201 in a grid box over Scandinavia ( $60-70^{\circ}\text{N}$ ,  $12.5-42.5^{\circ}\text{E}$ ) from that in a grid box over east-  
 202 ern Greenland ( $72.5-90^{\circ}\text{N}$ ,  $2.5-42.5^{\circ}\text{W}$ ). The MSLP in each grid box is cosine-weighted  
 203 to account for the convergence of meridians at higher latitudes. The two nodes, primar-  
 204 ily based on the track of a cyclone and the development of a Scandinavian ridge (see Fig-

205 ure 4), are shown as black dashed lines in Figure 3. The Ural high, also shown Figure  
 206 3, is defined as the area-average MSLP in the grid box 45-60°N, 50-80°E.

207 To discern the tropospheric drivers of the vertical wave flux, we assess the MSLP  
 208 evolutions of ECMWF ensemble members from 29 January and 1 February 2018 with  
 209 the top and bottom 10%-mean 300 hPa [ $v^*T^*$ ] for 4–6 February. Results (Figure 4) sup-  
 210 port the correlation analysis from Figure 3; a cyclone near Iceland on 3 February pro-  
 211 gresses up the eastern coast of Greenland and deepens to <970 hPa by 5 February in  
 212 the high-flux members, with a ridge extending from the Azores through Scandinavia, whilst  
 213 in the low-flux members the cyclone moves south-east towards Europe and weakens with-  
 214 out any ridge development. Figure 4c demonstrates the dipole structure; pressures are  
 215 >20 hPa higher (lower) over Scandinavia (Greenland) in the top 10% versus the bottom  
 216 10% heat flux members. A similar result is found when the same analysis is performed  
 217 in the NCEP forecasts (see Figure S2).

218 Next we compare the evolution of the S-G dipole with that of the Ural high (af-  
 219 ter Karpechko et al. (2018)) (Figure 5). The S-G dipole peaked at 52 hPa in ERA-Interim  
 220 on 5 February. There is rapid divergence after 3 February in accordance with Figure 4  
 221 (due to discrepancies in both nodes of the dipole), whilst it is also shown that the en-  
 222 semble members with the largest heat flux more closely follow ERA-Interim verification.  
 223 There is also a lagged relationship between the S-G dipole evolution and the Ural high,  
 224 and ensemble members with lowest mean 300 hPa heat flux lack both a strong S-G dipole  
 225 and Ural high. Inspecting potential vorticity (PV) on the 320 K isentropic surface in en-  
 226 semble members with the top 10% mean 300 hPa heat flux (Figure 6a) shows a tongue  
 227 of low PV air (<2 PVU) protruding polewards in the Atlantic sector east of Greenland  
 228 on 5 February before becoming cut-off and overturning on 8 February, indicative of an  
 229 anticyclonic Rossby wave break. This evolution is spatially and temporally coherent with  
 230 both the cyclone track/S-G dipole development and the 300 hPa heat flux. The wave  
 231 break is not present in ensemble members with the lowest 10% heat flux, which corre-  
 232 spondingly lacked a strong S-G dipole (Figure 6b). Thus, the predictability of the wave  
 233 breaking event and its impact on the stationary wave pattern indicates a possible expla-  
 234 nation for the abrupt forecast transition, as well as a dynamical mechanism by which  
 235 the S-G dipole in MSLP relates to both enhanced wave activity and amplification of the  
 236 Ural high downstream (through the attendant upper-level PV anomaly).

237 The relationship between the S-G dipole, the Ural high, and 300 hPa heat flux in  
 238 February 2018 is shown in Figure 7. Forecast heat flux increases approximately linearly  
 239 with S-G dipole strength ( $r = 0.79$  in NCEP vs.  $0.75$  in ECMWF) and heat flux is only  
 240 enhanced for values of the S-G dipole above  $\sim 40$  hPa. However, not all ensemble mem-  
 241 bers with an enhanced dipole produce enhanced heat flux; members with the strongest  
 242 heat flux feature both an amplified S-G dipole *and* a strengthened Ural high. Thus, the  
 243 enhancement of wave activity and amplification of the Ural high was dependent upon  
 244 the prior occurrence of the S-G dipole/wave breaking event as well as specifics of the wave  
 245 break and its interaction with the stratosphere. Figure 8 illustrates the surface evolu-  
 246 tion of the Ural high over 6–8 February in high vs. low heat flux members (c.f. Figure  
 247 4 and Figure S3). The anticyclone that develops over the Urals on 8 February in the high  
 248 heat flux members is the same system that is present over Scandinavia in the preced-  
 249 ing days associated with one node of the S-G dipole; this anticyclone is absent in the low  
 250 heat flux members, and thus directly links the evolution of the Ural high to the S-G dipole.  
 251 Therefore, the two precursors are not independent.

### 252 3.3 Historical S-G Dipoles

253 In this section we consider historical cases in extended-winter (November–March)  
 254 where the S-G dipole exceeds 40 hPa (similar in magnitude to the 2018 event, and ap-  
 255 proximately equal to the 99<sup>th</sup> percentile of daily November–March 1979-2017 ERA-Interim  
 256 climatology) to discern whether the dipole is a characteristic of previous cases of SPV  
 257 weakening. This threshold is not influenced by the time of year of an individual event,  
 258 as there is little day-to-day variability in the daily-mean and standard deviation of the  
 259 S-G dipole through the extended winter period. The Ural high is also considered, and  
 260 by using these previous examples we seek to understand whether the dipole or the Ural  
 261 high was the root cause of the enhanced vertical wave activity.

262 Motivated by Charlton and Polvani (2007) and their consideration of stratospheric  
 263 radiative timescales, we use a window of 20 days to separate individual events, yielding  
 264 a total of 49 cases (listed in Table S1). The strongest S-G dipole, 56 hPa, occurred on  
 265 15 March 2015. In Figure 9 we see the MSLP lag-composite anomaly evolution, with a  
 266 cyclone tracking up eastern Greenland into the Arctic region and a concomitant anti-  
 267 cyclone over Scandinavia. Notably the anticyclone is of greater persistence throughout  
 268 this period with transient amplification upon the passage of the cyclone. Following the

269 dipole peak, the anomaly field resembles the Scandinavian blocking Atlantic weather regime  
 270 (Cassou, Terray, Hurrell, & Deser, 2004; Charlton-Perez, Ferranti, & Lee, 2018) and is  
 271 similar to the precursors to weak SPV episodes shown in Kolstad and Charlton-Perez  
 272 (2011).

273 These historical events are also associated with anticyclonic wave breaking (Fig-  
 274 ure 10) similar to that which occurred in 2018, with the wave break in the Atlantic and  
 275 northern Europe evident through the reversal of the meridional PV gradient on the 315  
 276 K isentropic surface in this region. Composites of 45–75°N [ $v^*T^*$ ] and 60–90°N geopo-  
 277 tential height for 30 days before and after the peak of the dipole are shown in Figure 11.  
 278 Strong S-G dipoles are associated with a significant vertical wave pulse, and a weaken-  
 279 ing of the SPV (increasing polar cap geopotential heights indicating a negative strato-  
 280 spheric NAM tendency) in 10–15 days. It should be emphasized that these results show  
 281 relative vortex weakening, rather than the development of a climatologically weak vor-  
 282 tex. Indeed, some cases show a weakening of a strong SPV, or a temporary reduction  
 283 in the rate of vortex intensification, following an S-G dipole event. The evolution in 2018  
 284 (not shown) is very similar to the composites, albeit with increased magnitude.

285 To discern whether these historically strong S-G dipoles were also associated with  
 286 enhanced Ural highs, we analyse the change in the Ural high at a 3-day lag from the dipole  
 287 peak (motivated by the evolution in 2018). There is no clear tendency toward either a  
 288 strengthening or a weakening Ural high ( $\mu = 0.3$  hPa,  $\sigma = 10.3$  hPa). Splitting the com-  
 289 posites by whether the Ural high weakens or strengthens does not significantly alter the  
 290 composites: strong S-G dipoles followed by a weakening of the Ural high still show en-  
 291 hanced heat flux and a weakened polar vortex in the following days. This indicates it  
 292 is the wave break associated with the S-G dipole, not the resultant Ural high, which drives  
 293 the enhanced vertical wave flux - and that instead, in 2018, the Ural high was a conse-  
 294 quence of the preceding evolution.

295 Next, we assess the association between the S-G dipole and observed major mid-  
 296 winter SSWs prior to 2018 (Table 1). Of the 23 SSWs (Karpechko et al., 2017), we find  
 297 8 (35%) followed a similar evolution to 2018 and were preceded by an S-G dipole exceed-  
 298 ing 40 hPa within 15 days of the start date of the SSW. Given the total of 345 days pre-  
 299 ceding the 23 events (and assuming independence), this is 2.3 times larger than the cli-  
 300 matological likelihood (since 40 hPa is approximately the 99<sup>th</sup> percentile, it would be



301 expected that it was exceeded on 3-4 days). We note that the 2018 event was stronger  
 302 than any of these prior events associated with major SSWs (the previous strongest be-  
 303 ing 48 hPa preceding the major SSW in March 1981), possibly a facet of 2018 being the  
 304 event used to define the index. Although the major SSW in February 2018 was a vor-  
 305 tex split, 6 of the observed SSWs with a strong S-G dipole precursor were displacement  
 306 events (Karpechko et al., 2017) suggesting this pattern does not itself induce a specific  
 307 stratospheric evolution but acts to amplify an existing planetary wave structure. When  
 308 2018 is included, 78% of the major SSWs preceded by an amplified S-G dipole were downward-  
 309 propagating (Karpechko et al., 2017), with only March 1981 and February 2008 other-  
 310 wise. This is larger than the observed ratio of 57% (although the sample is too small to  
 311 draw robust conclusions), but is in agreement with Birner and Albers (2017) who note  
 312 larger tropospheric impacts following SSWs preceded by enhanced tropospheric wave ac-  
 313 tivity. We further note that 33% (90%) of the S-G dipole events considered here were  
 314 associated with daily 500 hPa [ $v^*T^*$ ] exceeding  $2\sigma$  ( $1\sigma$ ) within 5 days either side of the  
 315 events, indicating the dipole is an important contributor to anomalously high zonal-mean  
 316 tropospheric wave flux in general.

#### 317 **4 Discussion and Conclusions**

318 In this study we have shown that the abrupt onset of predictions of stratospheric  
 319 polar vortex (SPV) weakening and sudden stratospheric warming (SSW) in February 2018  
 320 was driven by an anticyclonic Rossby wave break (Figure 6) associated with the track  
 321 and intensity of a cyclone over eastern Greenland, and an associated ridge over Scan-  
 322 dinavia. From this, we define a Scandinavia-Greenland (S-G) dipole index in MSLP to  
 323 describe the evolution, and show that this was not well-forecast at long lead-times. The  
 324 location and intensity of the cyclone was a rare occurrence, with the mean MSLP in the  
 325 Greenland node and the dipole itself exceeding the 99th percentile of extended winter  
 326 months from 1979-2017. Occurrences of similarly strong S-G dipoles in reanalysis are shown  
 327 to be associated with anticyclonic wave breaking in the Atlantic sector (Figure 10), which  
 328 induces anomalously strong vertical wave activity (Figure 11a), and a rapid tendency  
 329 towards a weakened SPV/negative stratospheric NAM (Figure 11b) within 10 days. This  
 330 indicates that the evolution in 2018 was not a characteristic of the specific flow config-  
 331 uration but a more general mechanism for vortex weakening present in other events.

332 We have also shown that the S-G dipole and wave breaking event was important  
333 for amplifying a high pressure system over the Urals, first described in Karpechko et al.  
334 (2018) as a surface-pressure precursor of the 2018 SSW. Our results suggest that the Ural  
335 high was likely a consequence of the wave breaking event which drove stratospheric wave  
336 activity leading to the SSW, rather than a primary driver itself. The initial divergence  
337 in the evolution of the SPV strength and the onset of the enhanced vertical wave flux  
338 occurred around 5 February (Figure 2), preceding the amplification of the Ural high which  
339 followed on 8 February (Figure 5b), which further indicates the Ural high was a secondary  
340 response. It is likely that the persistence of the Ural high might have resulted in its de-  
341 tection in the averaging used in Karpechko et al. (2018), rather than the transience of  
342 the S-G dipole/wave break.

343 Our results differ from previous work through using a ‘bottom-up’ perspective, as-  
344 sessing the stratospheric response to tropospheric events. We provide a particular *tran-*  
345 *sient* trigger which would not be easily distinguished through ‘top-down’ time-mean com-  
346 posites (where the tropospheric configuration prior to stratospheric events is considered).  
347 This helps illuminate mechanisms by which persistent tropospheric blocking, including  
348 Scandinavian blocking which has previously been shown to precede SSWs (Cohen & Jones,  
349 2011; Kolstad & Charlton-Perez, 2011; Martius et al., 2009), can produce *sudden* changes  
350 in the stratospheric circulation. Furthermore, our results apply to a wider range of SPV  
351 variability than major SSWs – even the case of weakening a climatologically strong vor-  
352 tex towards an average state – which helps describe precursors of a larger proportion of  
353 the sub-seasonal behaviour. We therefore suggest the S-G dipole should be monitored  
354 operationally as a precursor to SPV weakening. Changes and uncertainty in its forecasts  
355 may help to qualitatively identify sources of uncertainty in stratospheric forecasts.

356 The intensity of the S-G dipole in 2018 was not well-forecast, driven by uncertainty  
357 in the track and intensity of an Atlantic cyclone. At longer lead-times, model biases in  
358 storm track and intensity may negatively impact the skill in predicting such events. For  
359 example, Frame, Methven, Roberts, and Titley (2015) showed cyclone intensity decayed  
360 with lead-time up to 15 days, which would constrain the ability of forecast models to pro-  
361 duce strong S-G dipoles sufficient for strong wave breaking and vortex weakening, whilst  
362 Gray, Dunning, Methven, Masato, and Chagnon (2014) and Saffin, Gray, Methven, and  
363 Williams (2017) also showed biases in tropopause PV and Rossby wave structure which  
364 may limit the ability to capture these types of wave breaking episodes and associated

365 stratospheric variability. These considerations are consistent with a deterministic limit  
 366 on SSW predictability (Karpechko, 2018; Taguchi, 2018).

367 The occurrence of strong S-G dipoles requires a poleward-shifted Atlantic storm  
 368 track, which is associated with the positive NAM/NAO pattern. This is often related  
 369 to the prior occurrence of a strengthened SPV (e.g. Baldwin & Dunkerton, 2001) and  
 370 SSWs are typically preceded by strong SPV conditions (e.g. Charlton & Polvani, 2007).  
 371 This behaviour could imply a two-way coupling in which the vortex drives its own vari-  
 372 ability - akin to a self-sustaining oscillator. Several studies (e.g. Lorenz & DeWeaver, 2007;  
 373 Tamarin & Kaspi, 2017) have indicated a poleward shift in the North Atlantic storm track  
 374 during winter under future climate change. This may lead to an increased frequency of  
 375 strong S-G dipoles and thus more frequent wave breaking events and stratospheric vor-  
 376 tex weakening, but the aforementioned biases may reduce the ability of climate models  
 377 to fully represent this source of sub-seasonal variability.

### 378 **Acknowledgments**

379 S.H.L. was funded by the Natural Environment Research Council (NERC) via the SCE-  
 380 NARIO Doctoral Training Partnership (NE/L002566/1) at the University of Reading.  
 381 S.J.W. was supported by the National Centre for Atmospheric Science, a NERC collab-  
 382 orative centre, under contract R8/H12/83/001. This work is based on S2S data, a joint  
 383 initiative of the World Weather Research Programme (WWRP) and the World Climate  
 384 Research Programme (WCRP). S2S and ERA-Interim reanalysis data are available on-  
 385 line at <https://apps.ecmwf.int/datasets/>. Pre-processing of data used here was completed  
 386 as part of the WCRP SPARC SNAP (Stratosphere-troposphere Processes and their Role  
 387 in Climate: Stratospheric Network for the Assessment of Predictability) programme. The  
 388 authors acknowledge three anonymous reviewers for their helpful suggestions.

### 389 **References**

- 390 Andrews, D., Holton, J., & Leovy, C. (1987). *Middle Atmosphere Dynamics*. Aca-  
 391 demic Press.
- 392 Attard, H. E., & Lang, A. L. (2019). Troposphere-stratosphere coupling follow-  
 393 ing tropospheric blocking and extratropical cyclones. *Monthly Weather Review*,  
 394 MWR-D-18-0335.1. doi: 10.1175/MWR-D-18-0335.1
- 395 Baldwin, M. P., & Dunkerton, T. J. (2001). Stratospheric harbingers of anomalous

- 396 weather regimes. *Science*, *294*(5542), 581–584. doi: 10.1126/science.1063315
- 397 Bao, M., Tan, X., Hartmann, D. L., & Ceppi, P. (2017). Classifying the tropo-  
 398 spheric precursor patterns of sudden stratospheric warmings. *Geophysical Re-  
 399 search Letters*, *44*(15), 8011–8016. doi: 10.1002/2017GL074611
- 400 Birner, T., & Albers, J. R. (2017). Sudden stratospheric warmings and anomalous  
 401 upward wave activity flux. *Sola*, *13A*(Special\_Edition), 8–12. doi: 10.2151/sola  
 402 .13a-002
- 403 Butler, A. H., Sjoberg, J. P., Seidel, D. J., & Rosenlof, K. H. (2017). A sudden  
 404 stratospheric warming compendium. *Earth System Science Data*, *9*(1), 63–76.  
 405 doi: 10.5194/essd-9-63-2017
- 406 Cassou, C., Terray, L., Hurrell, J. W., & Deser, C. (2004). North Atlantic winter cli-  
 407 mate regimes: spatial asymmetry, stationarity with time, and oceanic forcing.  
 408 *Journal of Climate*, *17*(5), 1055–1068. doi: 10.1175/1520-0442(2004)017<1055:  
 409 NAWCRS>2.0.CO;2
- 410 Charlton, A. J., & Polvani, L. M. (2007). A new look at stratospheric sudden warm-  
 411 ings. part i: climatology and modelling benchmarks. *J. Climate*, *20*(3), 449-  
 412 469. doi: 10.1175/JCLI3996.1
- 413 Charlton-Perez, A. J., Ferranti, L., & Lee, R. W. (2018). The influence of the strato-  
 414 spheric state on North Atlantic weather regimes. *Quarterly Journal of the  
 415 Royal Meteorological Society*, *144*(713), 1140–1151. doi: 10.1002/qj.3280
- 416 Cohen, J., & Jones, J. (2011). Tropospheric precursors and stratospheric warmings.  
 417 *Journal of Climate*, *25*(5), 1780–1790. doi: 10.1175/JCLI-D-11-00701.1
- 418 Colucci, S. J., & Kelleher, M. E. (2015). Diagnostic comparison of tropospheric  
 419 blocking events with and without sudden stratospheric warming. *Journal of  
 420 the Atmospheric Sciences*, *72*(6), 2227–2240. doi: 10.1175/jas-d-14-0160.1
- 421 Coy, L., Eckermann, S., & Hoppel, K. (2009). Planetary wave breaking and tropo-  
 422 spheric forcing as seen in the stratospheric sudden warming of 2006. *Journal of  
 423 the Atmospheric Sciences*, *66*(2), 495–507. doi: 10.1175/2008jas2784.1
- 424 Coy, L., & Pawson, S. (2014). The major stratospheric sudden warming of January  
 425 2013: analyses and forecasts in the GEOS-5 data assimilation system. *Monthly  
 426 Weather Review*, *143*(2), 491–510. doi: 10.1175/mwr-d-14-00023.1
- 427 Dee, D. P., Uppala, S. M., Simmons, A. J., Berrisford, P., Poli, P., Kobayashi, S., . . .  
 428 Vitart, F. (2011). The ERA-Interim reanalysis: configuration and performance

- 429 of the data assimilation system. *Quarterly Journal of the Royal Meteorological*  
 430 *Society*, *137*(656), 553–597. doi: 10.1002/qj.828
- 431 Ferranti, L., Magnusson, L., Vitart, F., & Richardson, D. (2018). A new prod-  
 432 uct to flag up the risk of cold spells in Europe weeks ahead. *ECMWF Newslet-*  
 433 *ter*(158), 1–8. doi: 10.21957/k2rlf88oe1
- 434 Frame, T. H. A., Methven, J., Roberts, N. M., & Titley, H. A. (2015). Predictability  
 435 of frontal waves and cyclones. *Weather and Forecasting*, *30*(5), 1291–1302. doi:  
 436 10.1175/waf-d-15-0039.1
- 437 Garfinkel, C. I., Hartmann, D. L., & Sassi, F. (2010). Tropospheric precursors  
 438 of anomalous northern hemisphere stratospheric polar vortices. *Journal of*  
 439 *Climate*, *23*(12), 3282–3299. doi: 10.1175/2010JCLI3010.1
- 440 Gray, S. L., Dunning, C. M., Methven, J., Masato, G., & Chagnon, J. M. (2014).  
 441 Systematic model forecast error in Rossby wave structure. *Geophysical Re-*  
 442 *search Letters*, *41*(8), 2979–2987. doi: 10.1002/2014GL059282
- 443 Julian, P. R., & Labitzke, K. B. (1965). A study of atmospheric energetics during  
 444 the January–February 1963 stratospheric warming. *Journal of the Atmospheric*  
 445 *Sciences*, *22*(6), 597–610. doi: 10.1175/1520-0469(1965)022<0597:asoaed>2.0.co;  
 446 2
- 447 Karpechko, A. Y. (2018). Predictability of sudden stratospheric warmings in the  
 448 ECMWF extended-range forecast system. *Monthly Weather Review*, *146*(4),  
 449 1063–1075. doi: 10.1175/MWR-D-17-0317.1
- 450 Karpechko, A. Y., Charlton-Perez, A., Balmaseda, T. N., Magdalena, & Vitart,  
 451 F. (2018). Predicting sudden stratospheric warming 2018 and its climate  
 452 impacts with a multimodel ensemble. *Geophysical Research Letters*, *45*(24),  
 453 13,538–13,546. doi: 10.1029/2018GL081091
- 454 Karpechko, A. Y., Hitchcock, P., Peters, D. H. W., & Schneidereit, A. (2017). Pre-  
 455 dictability of downward propagation of major sudden stratospheric warmings.  
 456 *Quarterly Journal of the Royal Meteorological Society*, *143*(704), 1459–1470.  
 457 doi: 10.1002/qj.3017
- 458 Kolstad, E. W., & Charlton-Perez, A. J. (2011). Observed and simulated precu-  
 459 sors of stratospheric polar vortex anomalies in the Northern Hemisphere. *Cli-*  
 460 *mate Dynamics*, *37*(7-8), 1443–1456. doi: 10.1007/s00382-010-0919-7
- 461 Krüger, K., Naujokat, B., & Labitzke, K. (2005). The unusual midwinter warming in

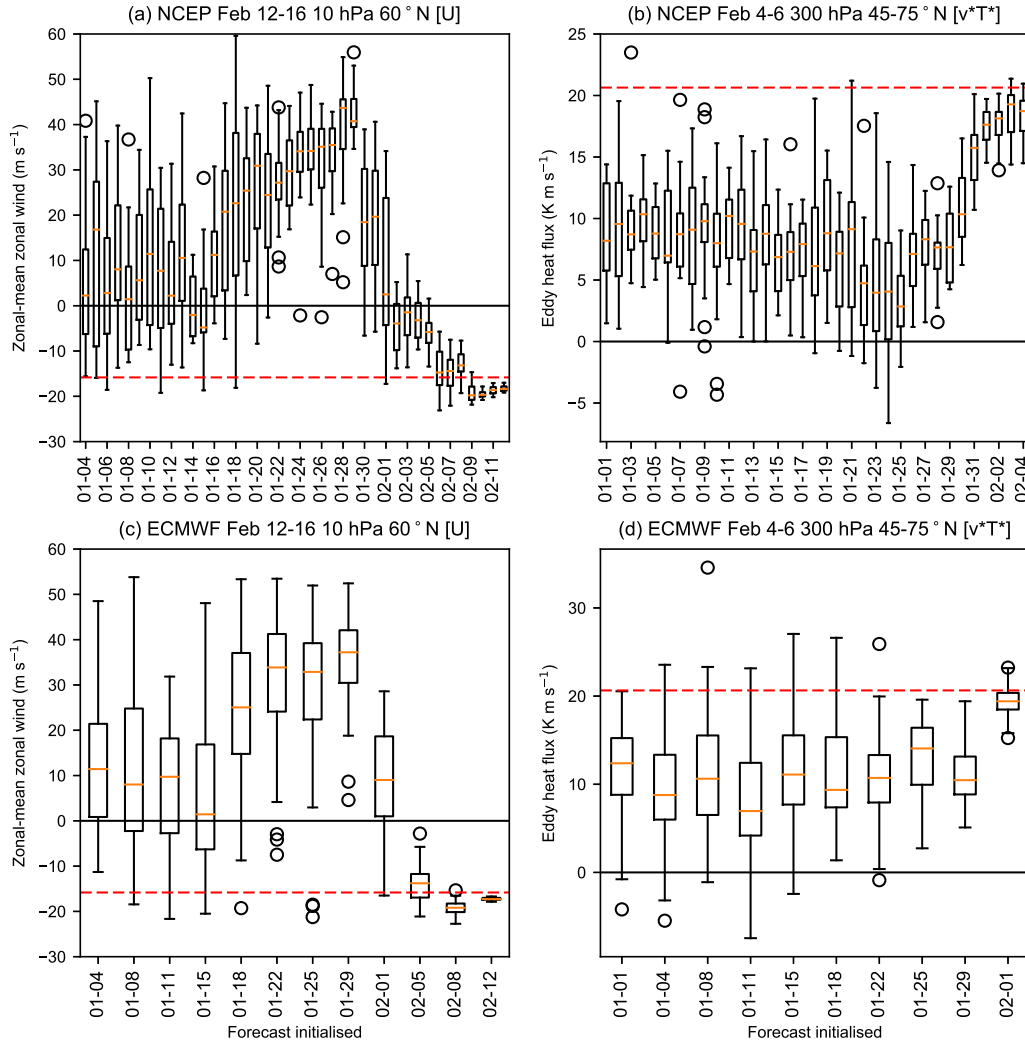
- 462 the Southern Hemisphere stratosphere 2002: a comparison to Northern Hemi-  
 463 sphere phenomena. *Journal of the Atmospheric Sciences*, *62*(3), 603–613. doi:  
 464 10.1175/jas-3316.1
- 465 Lorenz, D. J., & DeWeaver, E. T. (2007). Tropopause height and zonal wind re-  
 466 sponse to global warming in the IPCC scenario integrations. *Journal of Geo-*  
 467 *physical Research Atmospheres*, *112*(10), 1–11. doi: 10.1029/2006JD008087
- 468 Martius, O., Polvani, L. M., & Davies, H. C. (2009). Blocking precursors to strato-  
 469 spheric sudden warming events. *Geophysical Research Letters*, *36*(14), 1–5. doi:  
 470 10.1029/2009GL038776
- 471 O’Neill, A., Oatley, C. L., Charlton-Perez, A. J., Mitchell, D. M., & Jung, T. (2017).  
 472 Vortex splitting on a planetary scale in the stratosphere by cyclogenesis on a  
 473 subplanetary scale in the troposphere. *Quarterly Journal of the Royal Meteorolo-*  
 474 *logical Society*, *143*(703), 691–705. doi: 10.1002/qj.2957
- 475 Peings, Y. (2019). Ural blocking as a driver of early winter stratospheric warmings.  
 476 *Geophysical Research Letters*, 2019GL082097. doi: 10.1029/2019GL082097
- 477 Quiroz, R. S. (1986). The association of stratospheric warmings with tropo-  
 478 spheric blocking. *Journal of Geophysical Research*, *91*(D4), 5277. doi:  
 479 10.1029/jd091id04p05277
- 480 Saffin, L., Gray, S. L., Methven, J., & Williams, K. D. (2017). Processes maintaining  
 481 tropopause sharpness in numerical models. *Journal of Geophysical Research:*  
 482 *Atmospheres*, *122*(18), 9611–9627. doi: 10.1002/2017JD026879
- 483 Taguchi, M. (2014). Predictability of major stratospheric sudden warmings of the  
 484 vortex split type: case study of the 2002 southern event and the 2009 and 1989  
 485 northern events. *Journal of the Atmospheric Sciences*, *71*(8), 2886–2904. doi:  
 486 10.1175/jas-d-13-078.1
- 487 Taguchi, M. (2018). Comparison of subseasonal-to-seasonal model forecasts for  
 488 major stratospheric sudden warmings. *Journal of Geophysical Research: Atmo-*  
 489 *spheres*, *123*(18), 10,231–10,247. doi: 10.1029/2018JD028755
- 490 Tamarin, T., & Kaspi, Y. (2017). The poleward shift of storm tracks under global  
 491 warming: a Lagrangian perspective. *Geophysical Research Letters*, *44*(20),  
 492 10,666–10,674. doi: 10.1002/2017GL073633
- 493 Thompson, D. W., & Wallace, J. M. (2000). Annular modes in the extratropical cir-  
 494 culation. Part I: month-to-month variability. *Journal of Climate*, *13*(5), 1000–

- 495 1016. doi: 10.1175/1520-0442(2000)013<1000:AMITEC>2.0.CO;2
- 496 Tripathi, O. P., Baldwin, M., Charlton-Perez, A., Charron, M., Cheung, J. C. H.,  
497 Eckermann, S. D., . . . Stockdale, T. (2016). Examining the predictabil-  
498 ity of the stratospheric sudden warming of January 2013 using multi-  
499 ple NWP systems. *Monthly Weather Review*, *144*(5), 1935–1960. doi:  
500 10.1175/MWR-D-15-0010.1
- 501 Tripathi, O. P., Baldwin, M., Charlton-Perez, A., Charron, M., Eckermann, S. D.,  
502 Gerber, E., . . . Son, S. W. (2015). The predictability of the extratropical  
503 stratosphere on monthly time-scales and its impact on the skill of tropospheric  
504 forecasts. *Quarterly Journal of the Royal Meteorological Society*, *141*(689),  
505 987–1003. doi: 10.1002/qj.2432
- 506 Vitart, F., Ardilouze, C., Bonet, A., Brookshaw, A., Chen, M., Codorean, C., . . .  
507 Zhang, L. (2017). The subseasonal to seasonal (S2S) prediction project  
508 database. *Bulletin of the American Meteorological Society*, *98*(1), 163–173.  
509 doi: 10.1175/BAMS-D-16-0017.1
- 510 White, I., Garfinkel, C. I., Gerber, E. P., Jucker, M., Aquila, V., & Oman, L. D.  
511 (2019). The downward influence of sudden stratospheric warmings: associa-  
512 tion with tropospheric precursors. *Journal of Climate*, *32*(1), 85–108. doi:  
513 10.1175/JCLI-D-18-0053.1

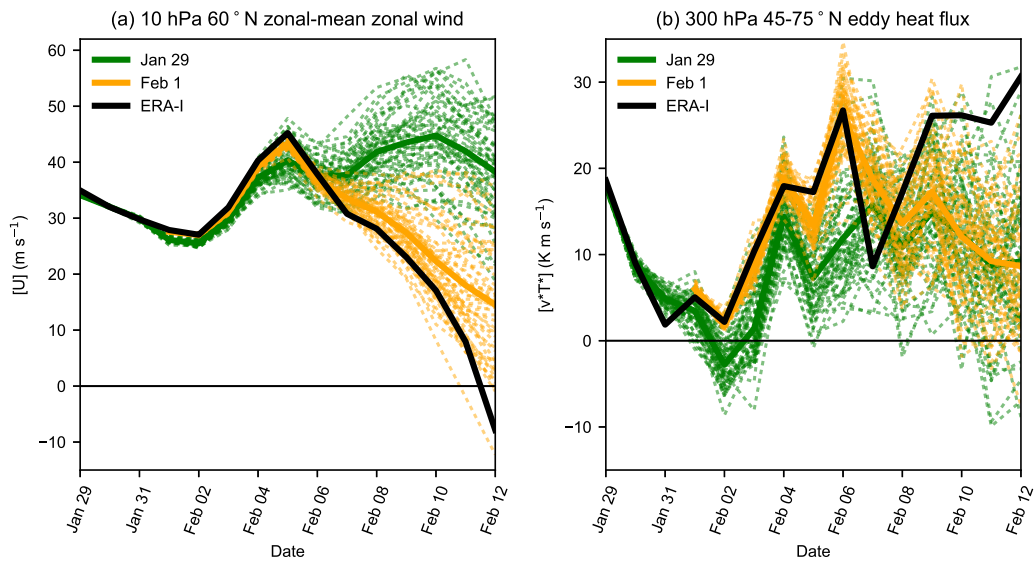
514 **Table 1.** Major SSWs in the period 1979–2017 (following Karpechko et al. (2017)) and the  
 515 peak value of the S-G dipole in the 15 days before the event according to ERA-Interim reanaly-  
 516 sis. Those events exceeding 40 hPa are shown in bold.

SSW event	Peak S-G index (hPa)
<b>February 1979</b>	<b>41</b>
<b>February 1980</b>	<b>43</b>
<b>March 1981</b>	<b>48</b>
December 1981	13
<b>February 1984</b>	<b>45</b>
<b>January 1985</b>	<b>44</b>
<b>January 1987</b>	<b>43</b>
December 1987	26
March 1988	21
February 1989	39
December 1998	34
February 1999	18
March 2000	24
February 2001	31
December 2001	24
January 2003	2
January 2004	12
<b>January 2006</b>	<b>42</b>
February 2007	17
<b>February 2008</b>	<b>40</b>
January 2009	22
February 2010	36
January 2013	27

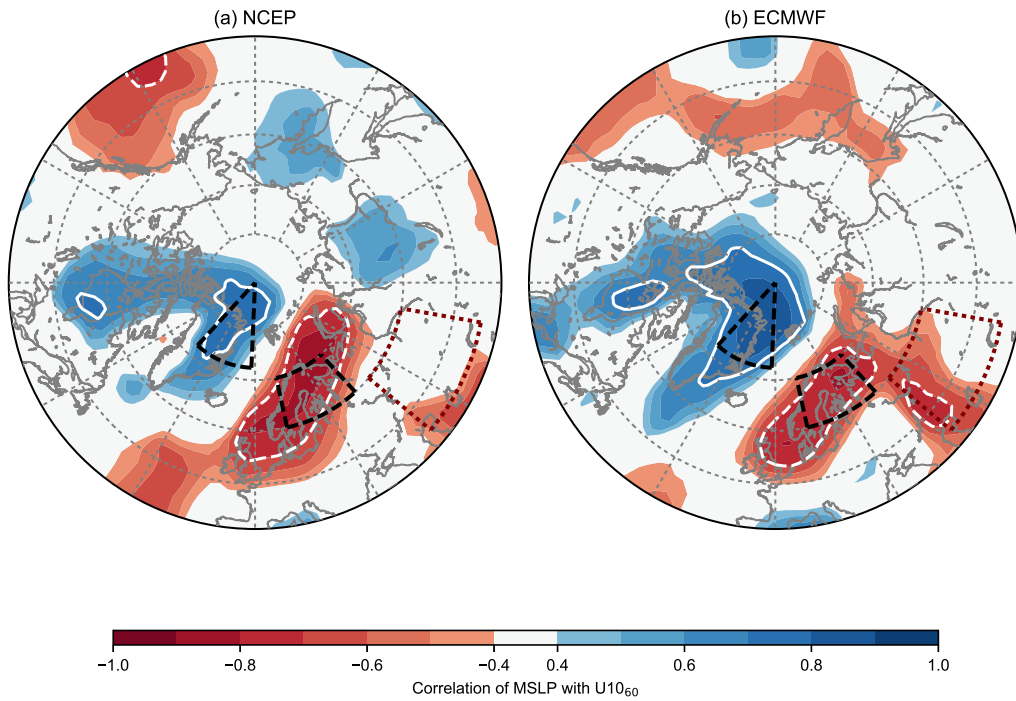




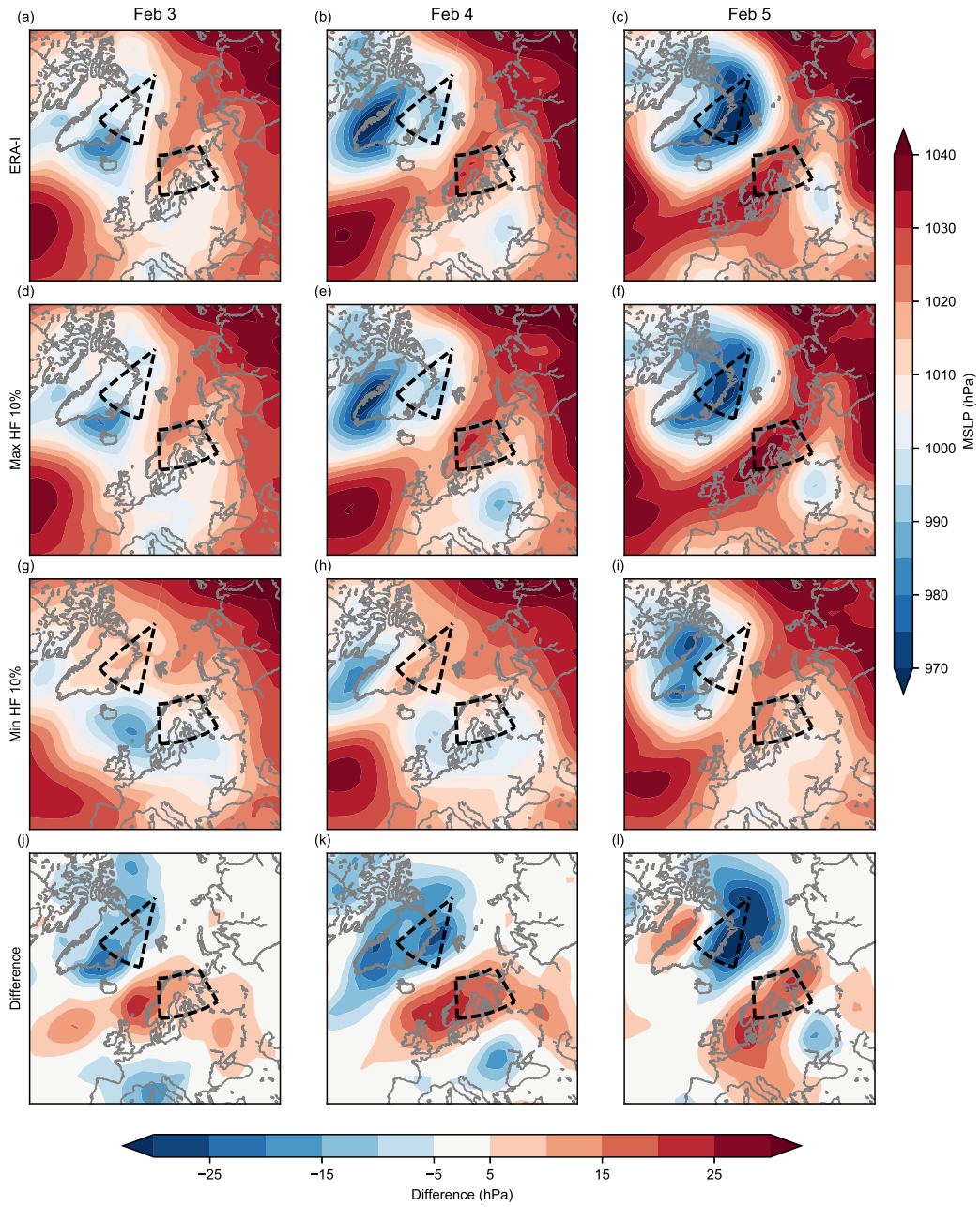
517 **Figure 1.** Boxplots showing (a), (c) average 10 hPa 60°N zonal-mean zonal-winds for 12–16  
 518 February 2018 and (b), (d) 300 hPa 45–75°N meridional eddy heat flux averaged over 4–6 Febru-  
 519 ary 2018 in (a), (b) NCEP and (c), (d) ECMWF models for all ensemble members as a function  
 520 of initialisation date. Boxes indicate the interquartile range (IQR), whiskers extend to the last  
 521 point less or greater than 1.5 times the IQR, with circles indicating outliers. The dashed red lines  
 522 indicate verifying values according to ERA-Interim reanalysis.



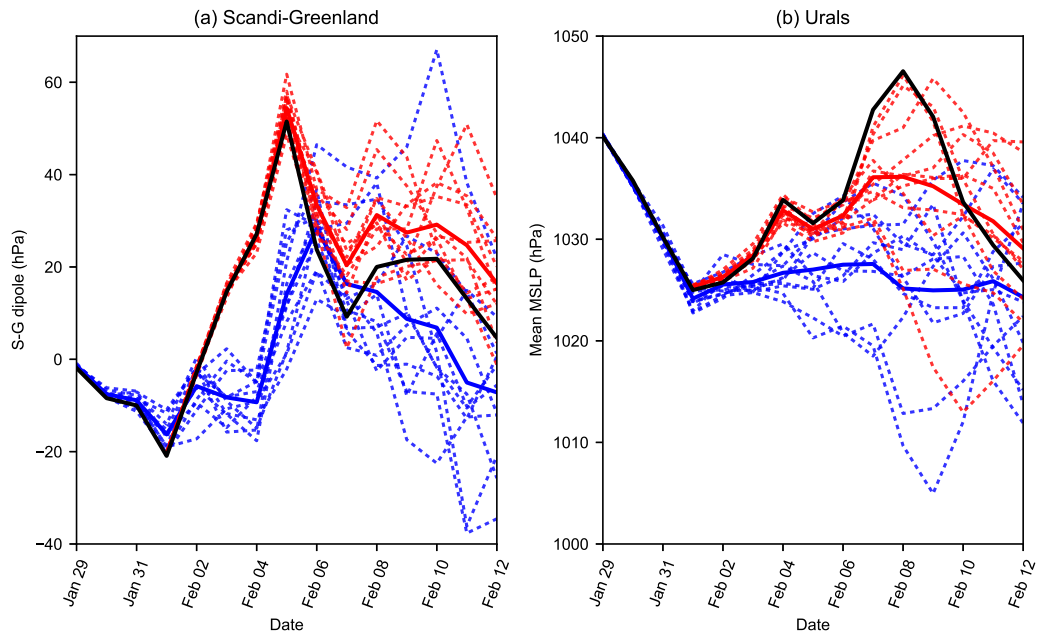
523 **Figure 2.** ECMWF ensemble forecasts from 29 January (dashed green) and 1 February  
 524 (dashed orange) for (a) 10 hPa 60°N zonal-mean zonal wind and (b) 300 hPa 45–75°N meridional  
 525 eddy heat flux for 29 January–12 February 2018. Ensemble means are shown with thick lines.  
 526 Verifying evolution from ERA-Interim is shown with the thick black line.



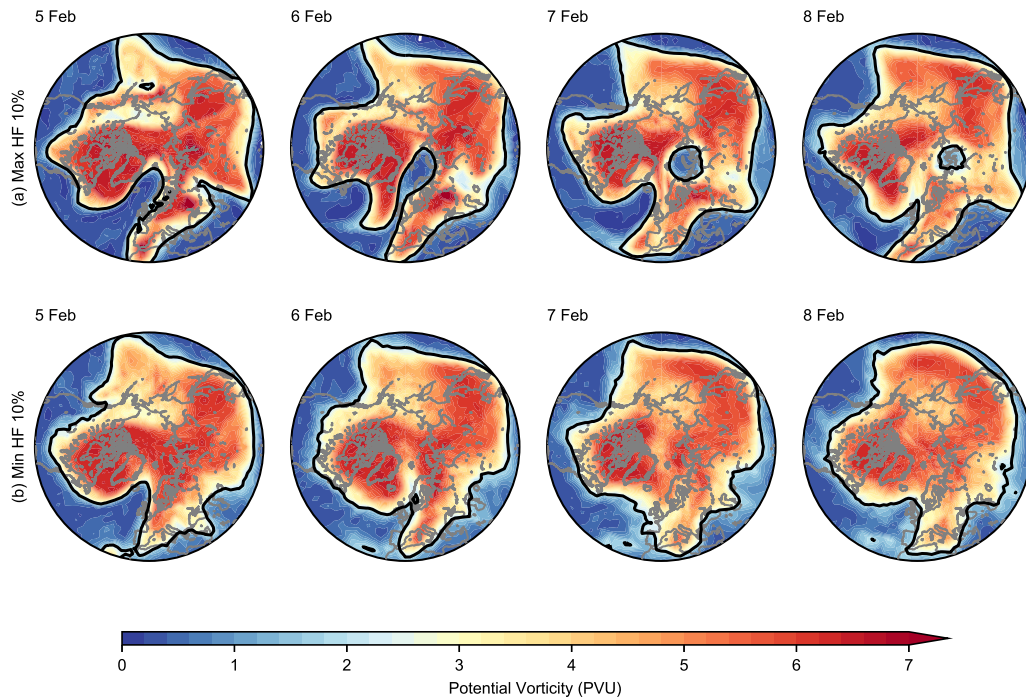
527 **Figure 3.** Linear correlation between average 9–11 February U10<sub>60</sub> and average 3–5 February  
 528 mean MSLP from (a) 29 January to 1 February NCEP forecasts and (b) 29 January and 1 Febru-  
 529 ary ECMWF forecasts. White lines delineate where the magnitude of the correlation exceeds 0.7.  
 530 The two nodes of the S-G dipole are shown with black dashed lines, and the location of the Ural  
 531 high is shown with maroon dotted lines.



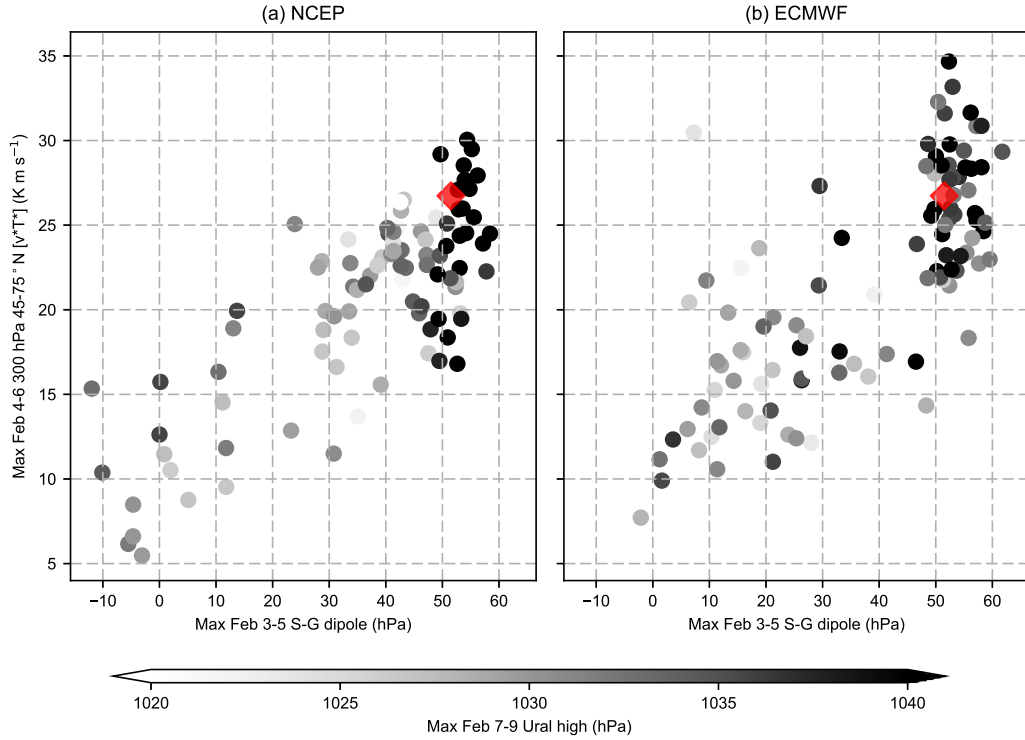
532 **Figure 4.** MSLP for 3–5 February from (a–c) ERA-Interim reanalysis, (d–f) the mean forecast  
 533 from members of the ECMWF 29 January and 1 February joined ensemble with the top 10% 300  
 534 hPa 45–75°N heat flux on 4–6 February, (g–i) the bottom 10%, and (j–l) the difference (d–f – g–i).  
 535 The two nodes of the S–G dipole are shown with black dashed lines.



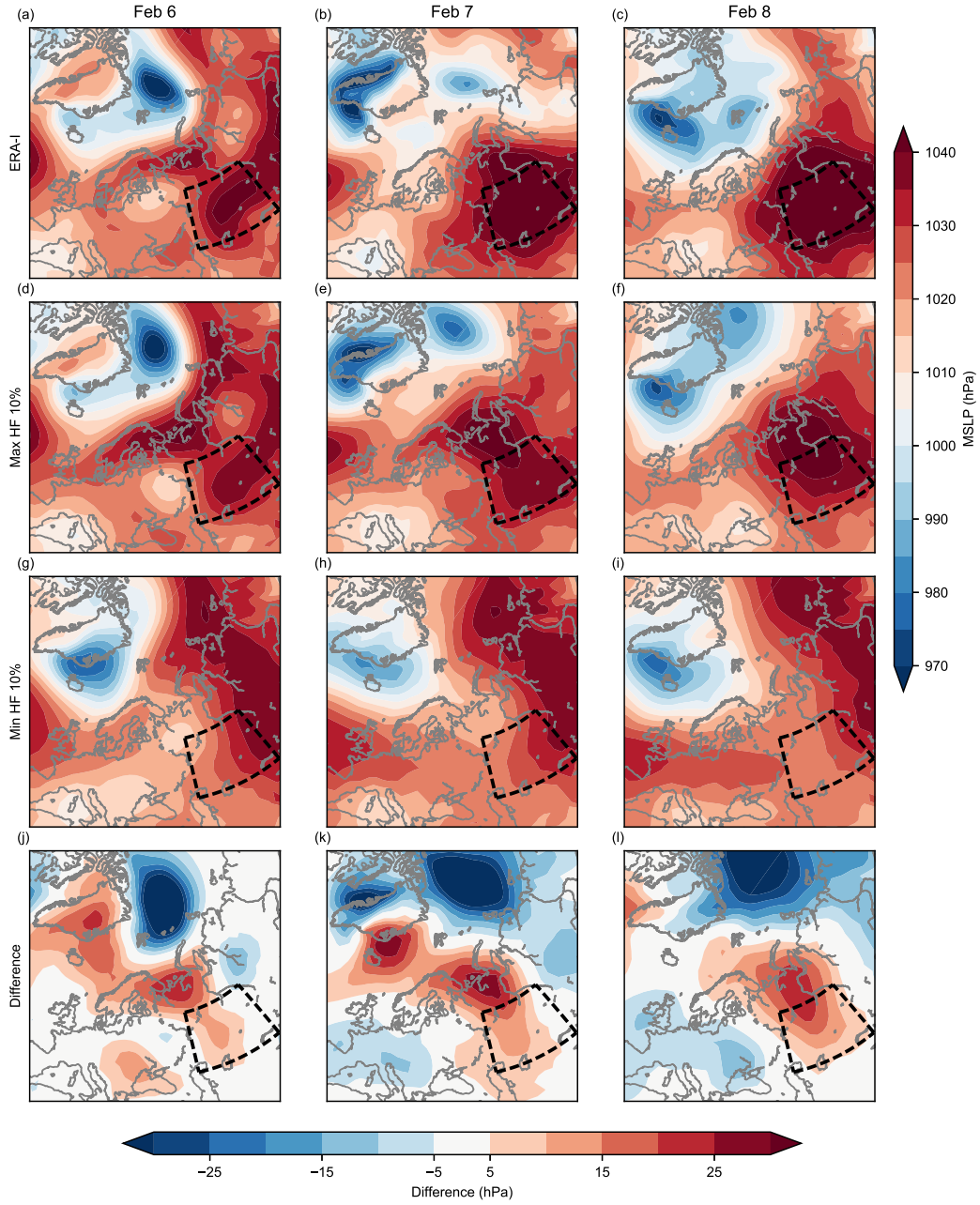
536 **Figure 5.** Time series of ECMWF ensemble forecasts from 29 January 1 February for (a) the  
 537 S-G dipole and (b) the Ural high from members with the top (dotted red) and bottom (dotted  
 538 blue) 10% mean 4–6 February 300 hPa 45–75°N [ $v \cdot T^*$ ]. Their respective means are shown with  
 539 thick lines coloured accordingly. The verifying evolution from ERA-Interim is shown in black.



540 **Figure 6.** Forecasts of PV on the 320 K isentropic surface for 5–8 February from members  
 541 of the ECMWF 29 January and 1 February joined ensemble. (a) shows the mean forecast from  
 542 members with the top 10% 300 hPa 45–75°N heat flux on 4–6 February and (b) the bottom 10%.  
 543 The 2 PV unit isoline (PVU, where  $1 \text{ PVU} = 10^{-6} \text{ m}^2 \text{ s}^{-1} \text{ K kg}^{-1}$ ) is contoured in black.

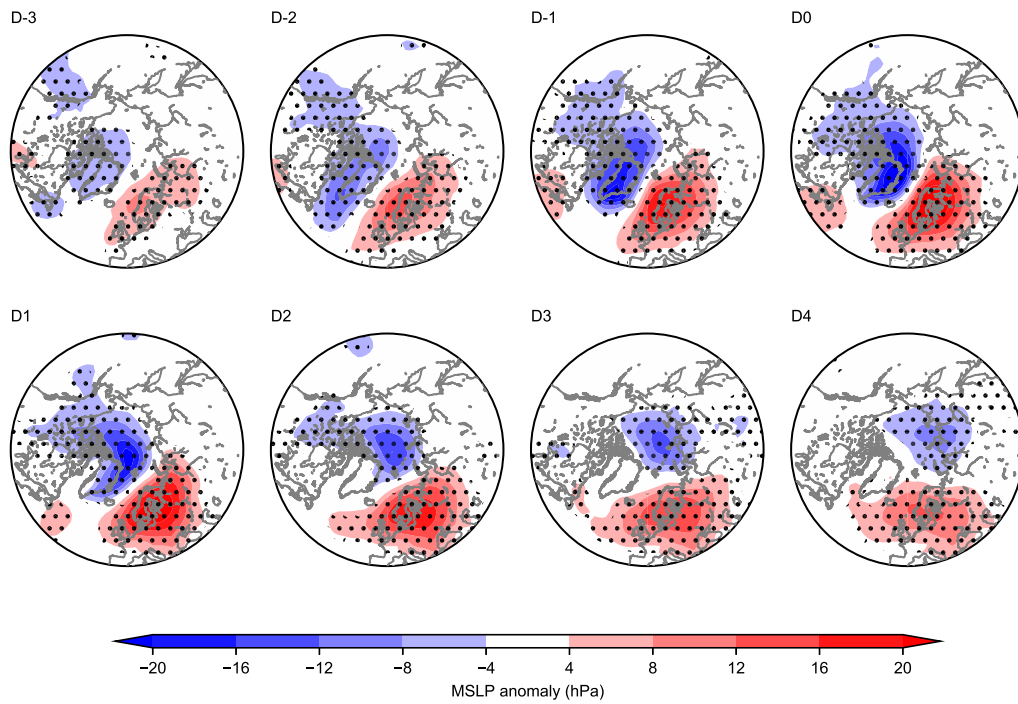


544 **Figure 7.** Scatter plots of maximum 4–6 February 300 hPa  $[v^*T^*]$  versus maximum 3–5  
 545 February mean S-G dipole for (a) NCEP ensembles from 29 January to 3 February ( $n = 96$ ), and  
 546 (b) ECMWF ensembles from 29 January and 1 February ( $n = 102$ ). The points are coloured by  
 547 the corresponding maximum 7–9 February Ural high strength. The verifying ERA-Interim value  
 548 is shown with a red diamond.

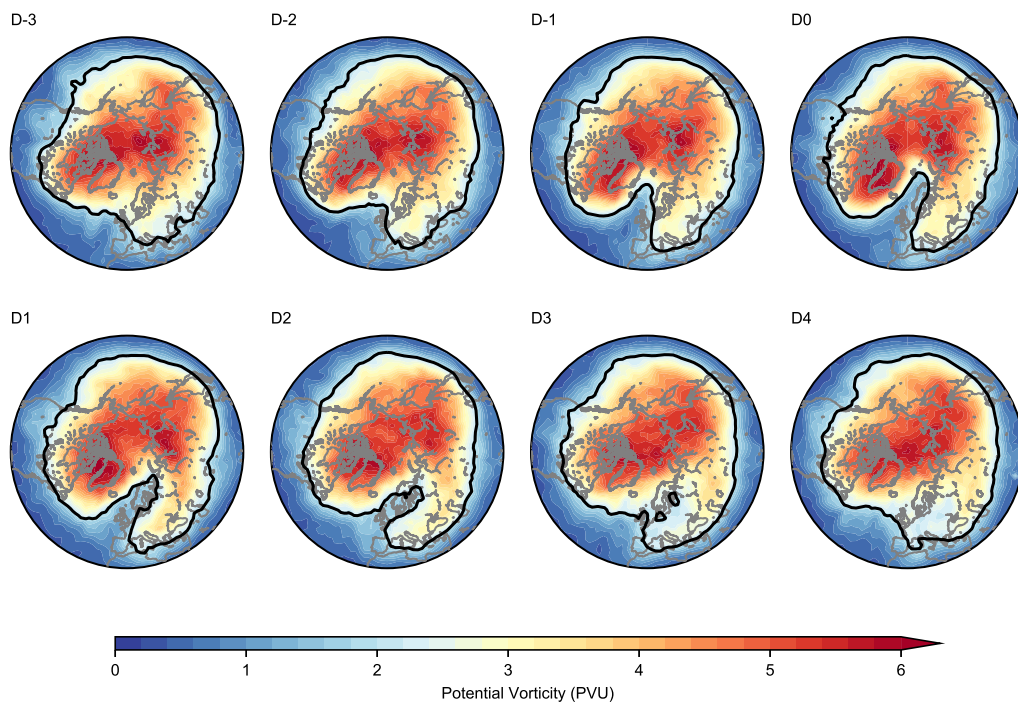


549 **Figure 8.** As in Figure 4 but for 6–8 February. The Ural high is indicated with black dashed  
 550 lines.

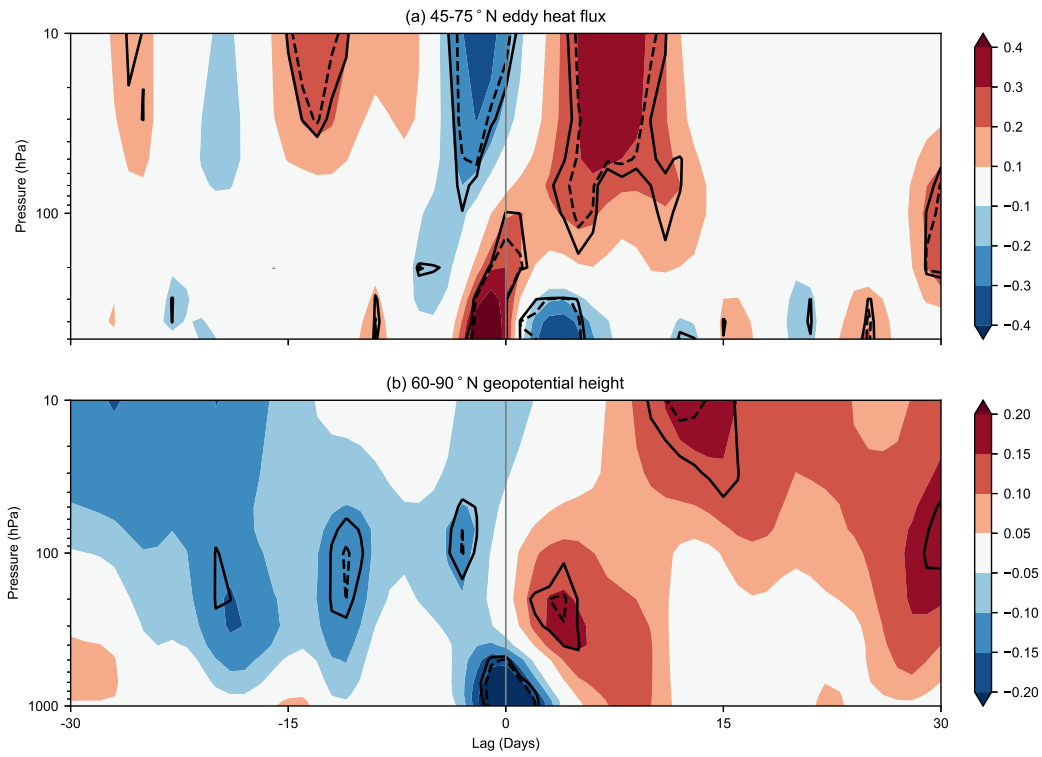




551 **Figure 9.** Composite of MSLP anomalies (with respect to January 1979–March 2017 clima-  
 552 tology) from ERA-Interim for the period 3 days before to 4 days after 49 historical S-G dipole  
 553 events exceeding 40 hPa. Stippling indicates areas significant at the 95% confidence level (for  
 554 details see Section 2).



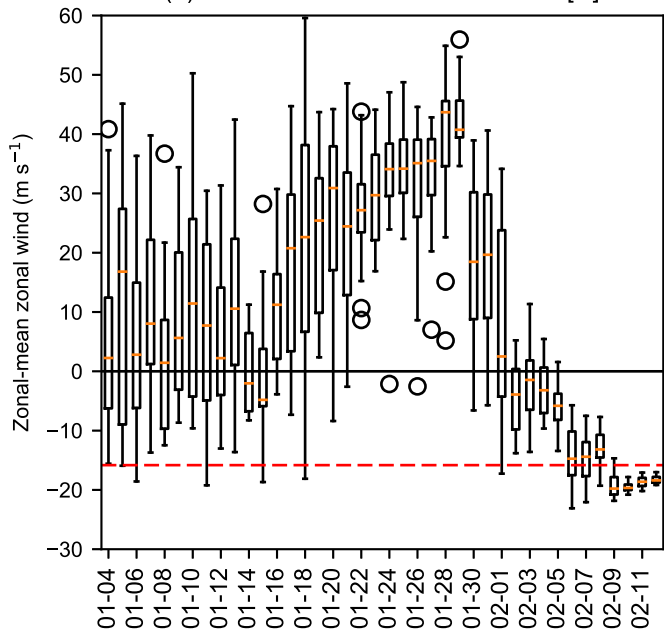
555 **Figure 10.** As in Figure 9 but for PV on the 315 K isentropic surface. The thick black line  
556 indicates the 2 PVU contour.



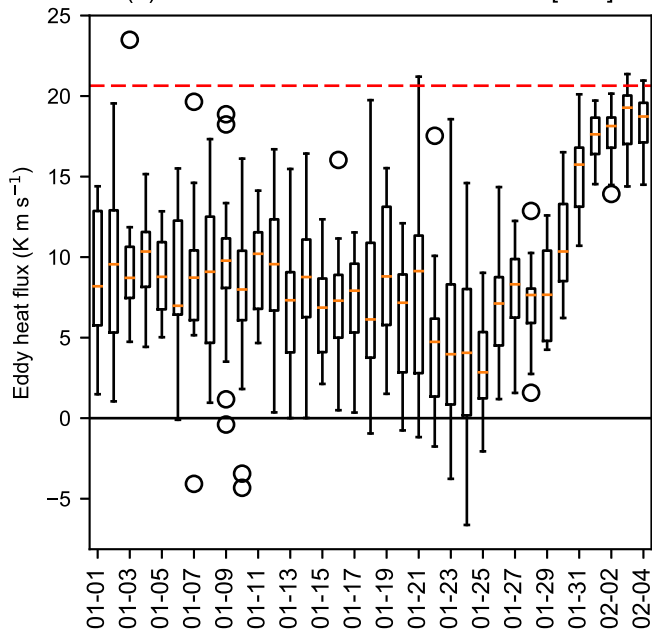
557 **Figure 11.** Composite of anomalies in (a) 45–75°N meridional eddy heat flux [ $v^*T^*$ ] and (b)  
 558 60–90°N geopotential height for 30 days before and after 49 events in ERA-Interim 1979–2017  
 559 where the S-G dipole exceeded 40 hPa. Anomalies are standardized departures and are filtered  
 560 using a  $1\sigma$  Gaussian smoother; in (b) these are shown relative to the mean for the 61-day win-  
 561 dow to show relative tendency. The gray vertical line indicates the day on which the 40 hPa  
 562 threshold was exceeded. Solid (dashed) black contours indicate regions significant at the 90%  
 563 (95%) confidence level (for details see Section 2).

Figure 1.

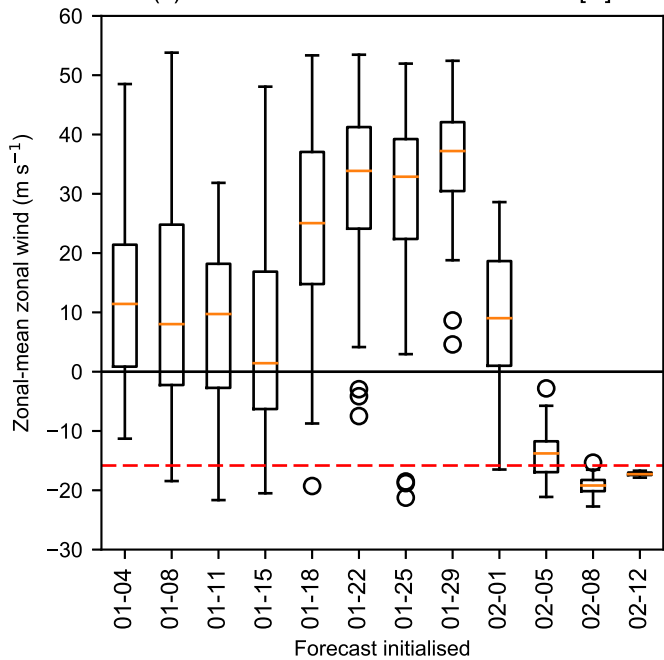
(a) NCEP Feb 12-16 10 hPa 60° N [U]



(b) NCEP Feb 4-6 300 hPa 45-75° N [v\*T\*]



(c) ECMWF Feb 12-16 10 hPa 60° N [U]



(d) ECMWF Feb 4-6 300 hPa 45-75° N [v\*T\*]

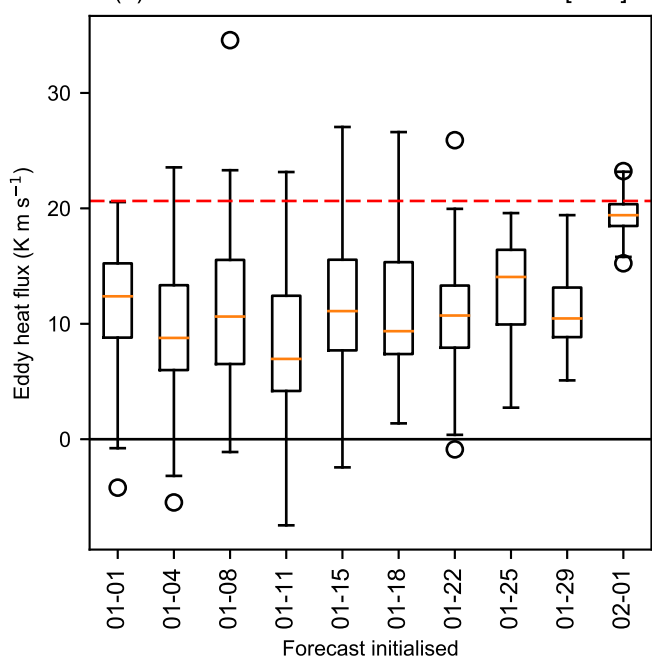
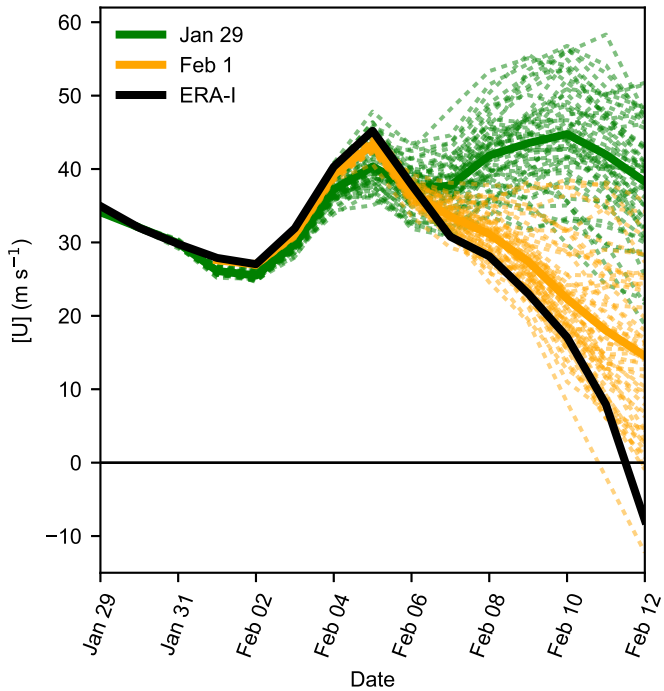


Figure 2.

(a) 10 hPa 60° N zonal-mean zonal wind



(b) 300 hPa 45-75° N eddy heat flux

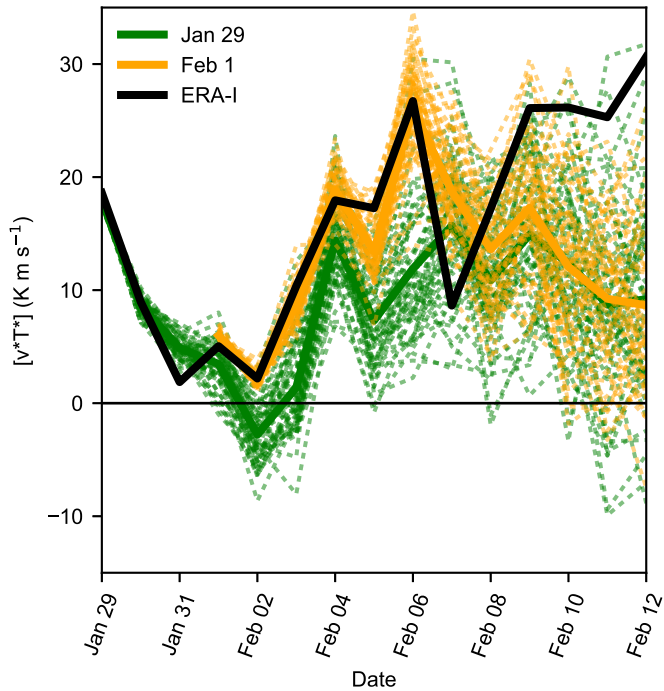
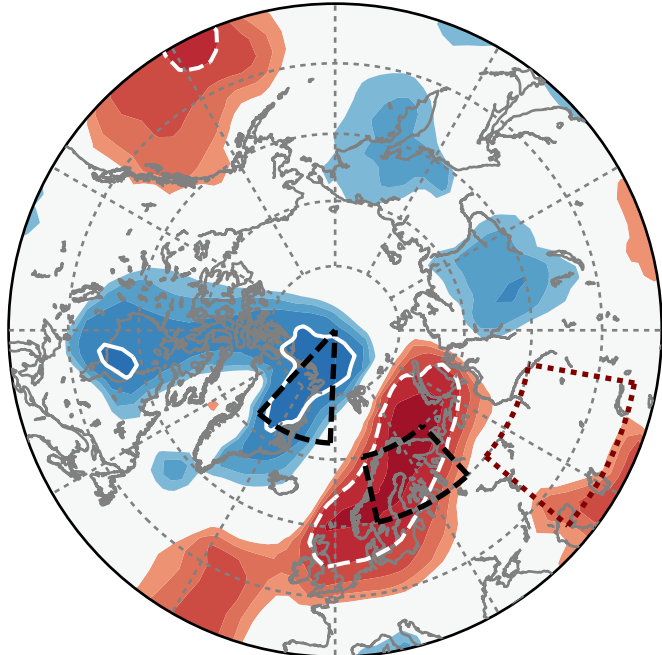


Figure 3.



(a) NCEP



(b) ECMWF

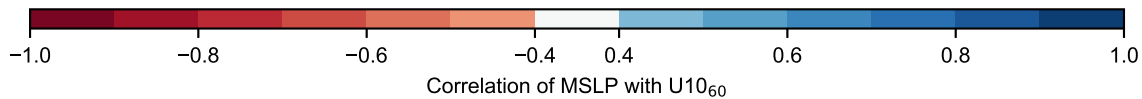
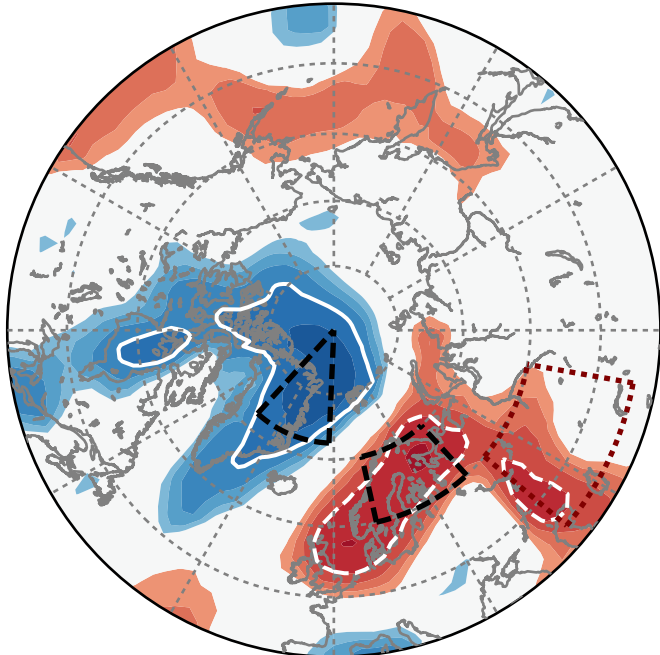


Figure 4.

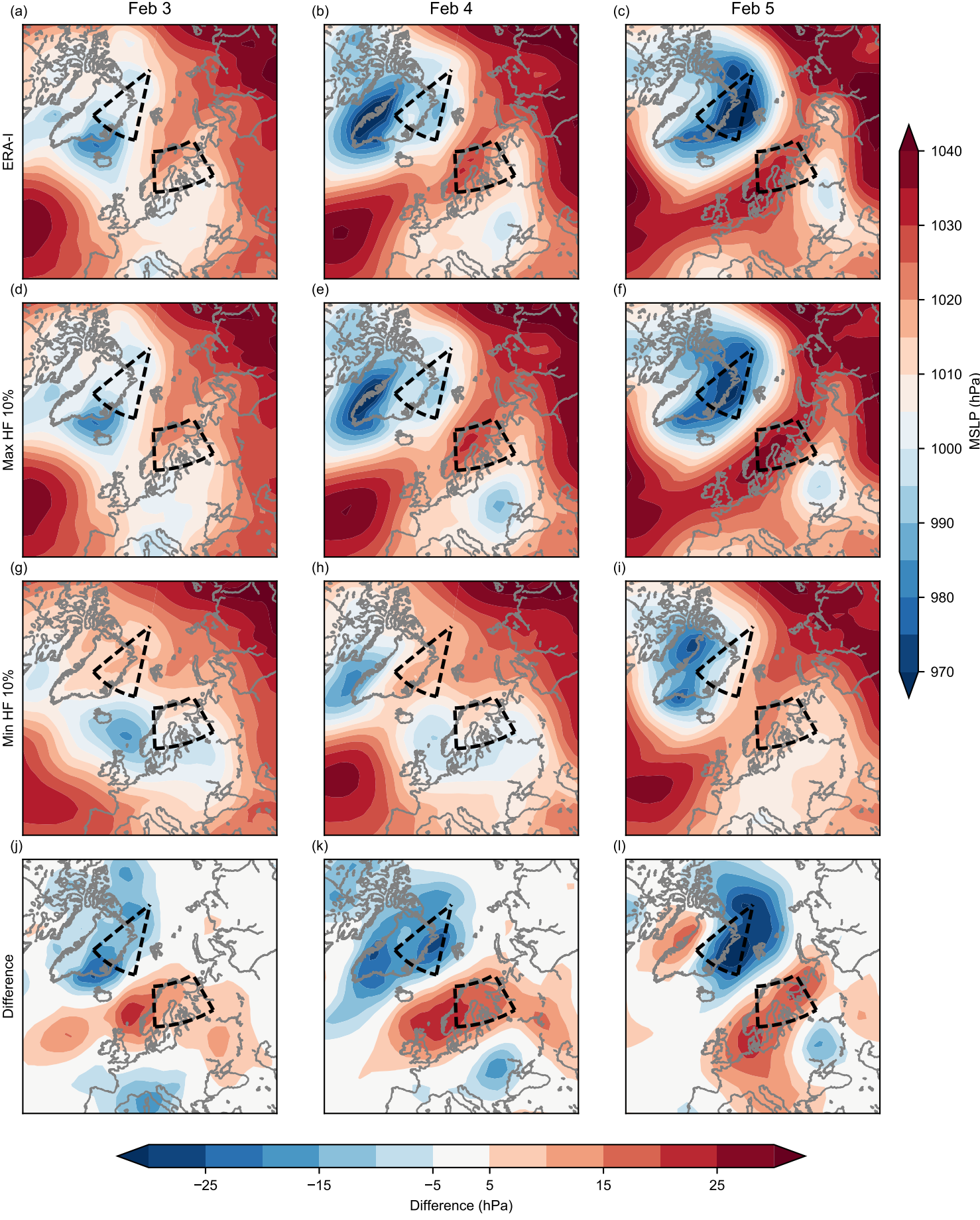
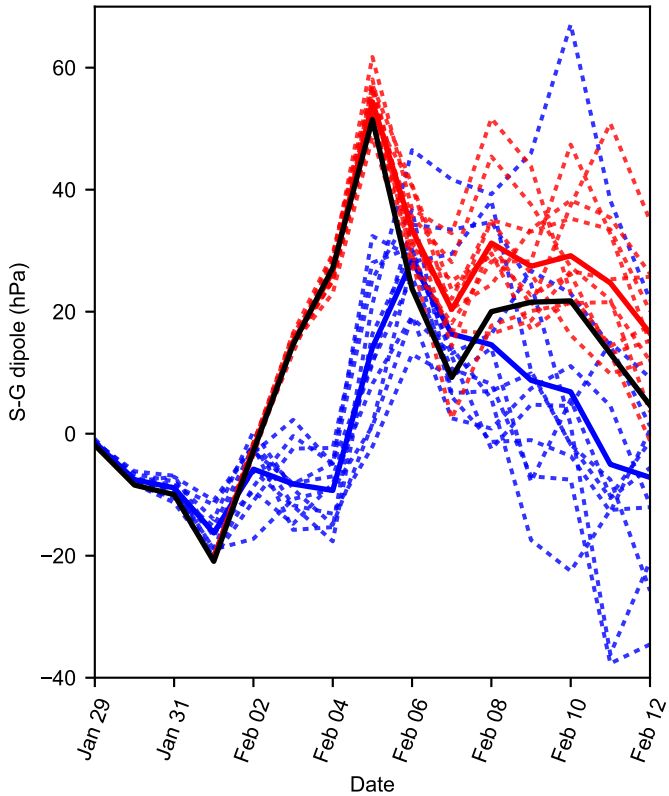


Figure 5.

(a) Scandi-Greenland



(b) Urals

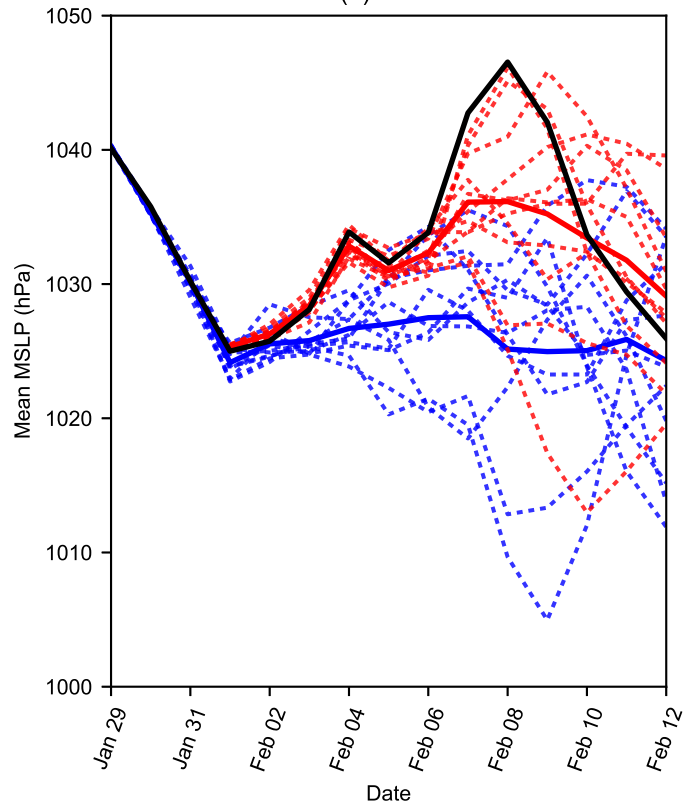


Figure 6.

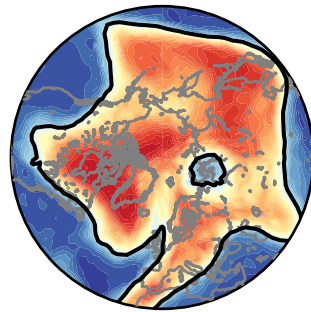
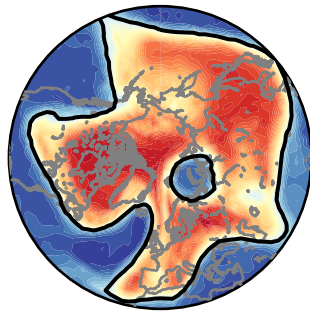
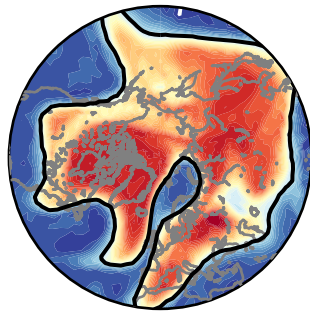
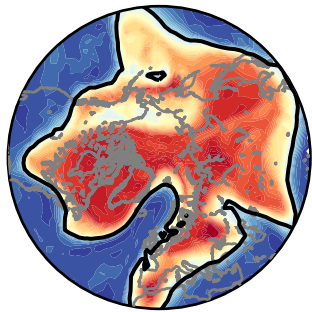
5 Feb

6 Feb

7 Feb

8 Feb

(a) Max HF 10%



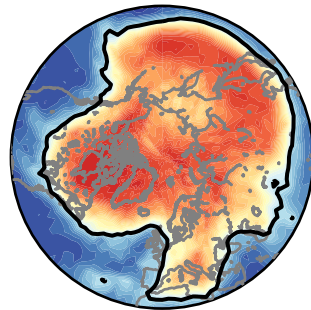
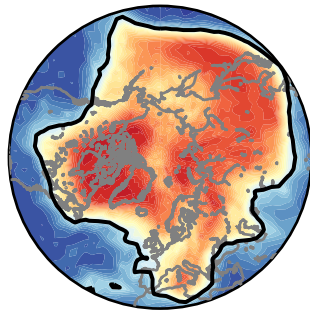
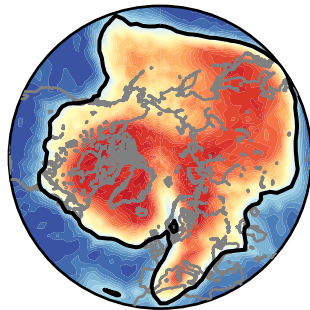
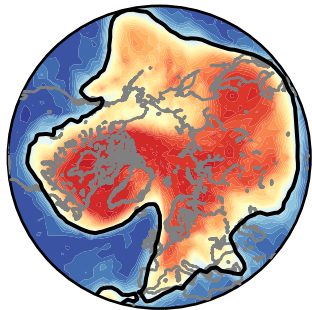
5 Feb

6 Feb

7 Feb

8 Feb

(b) Min HF 10%



Potential Vorticity (PVU)

Figure 7.



(a) NCEP

(b) ECMWF

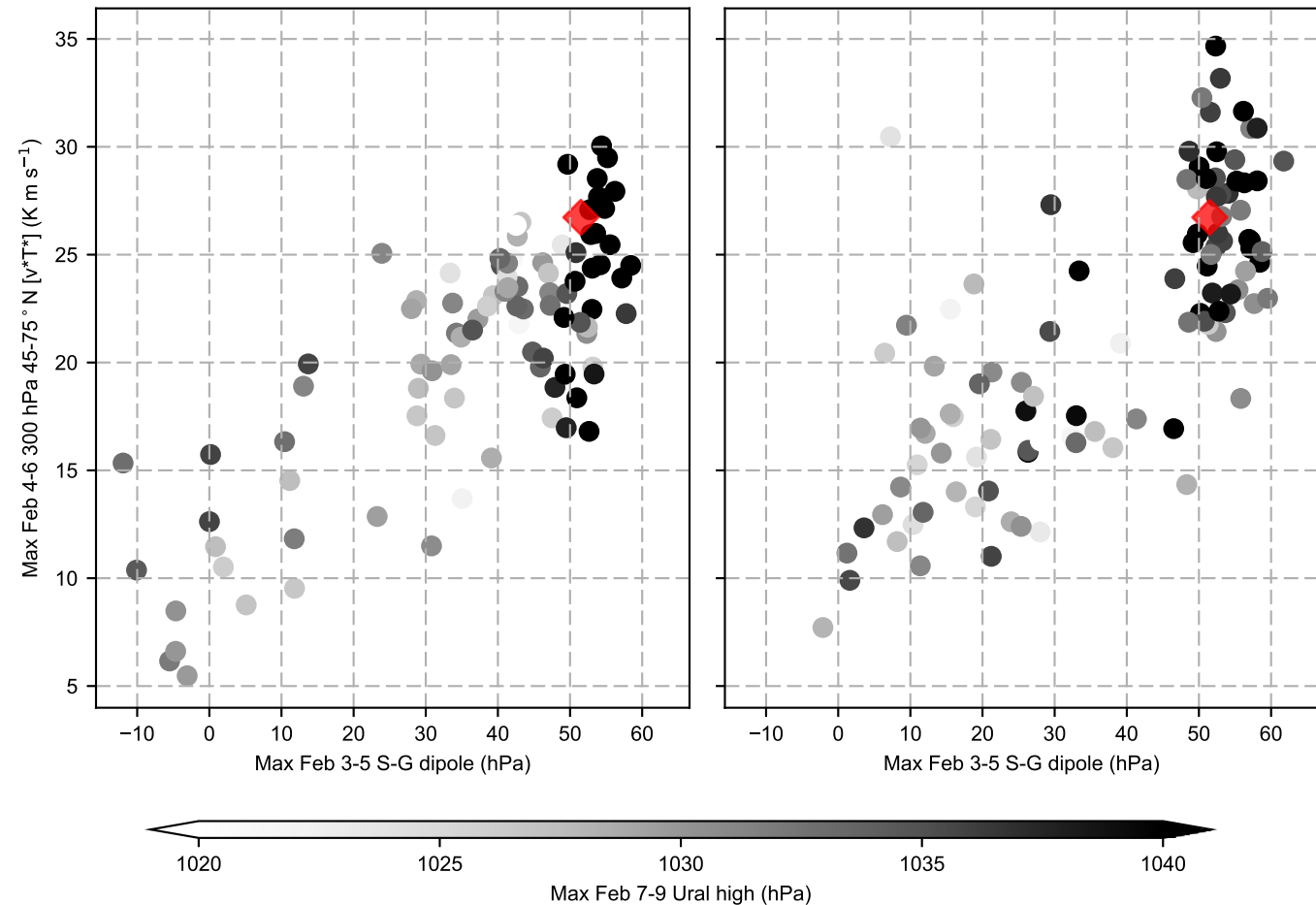


Figure 8.

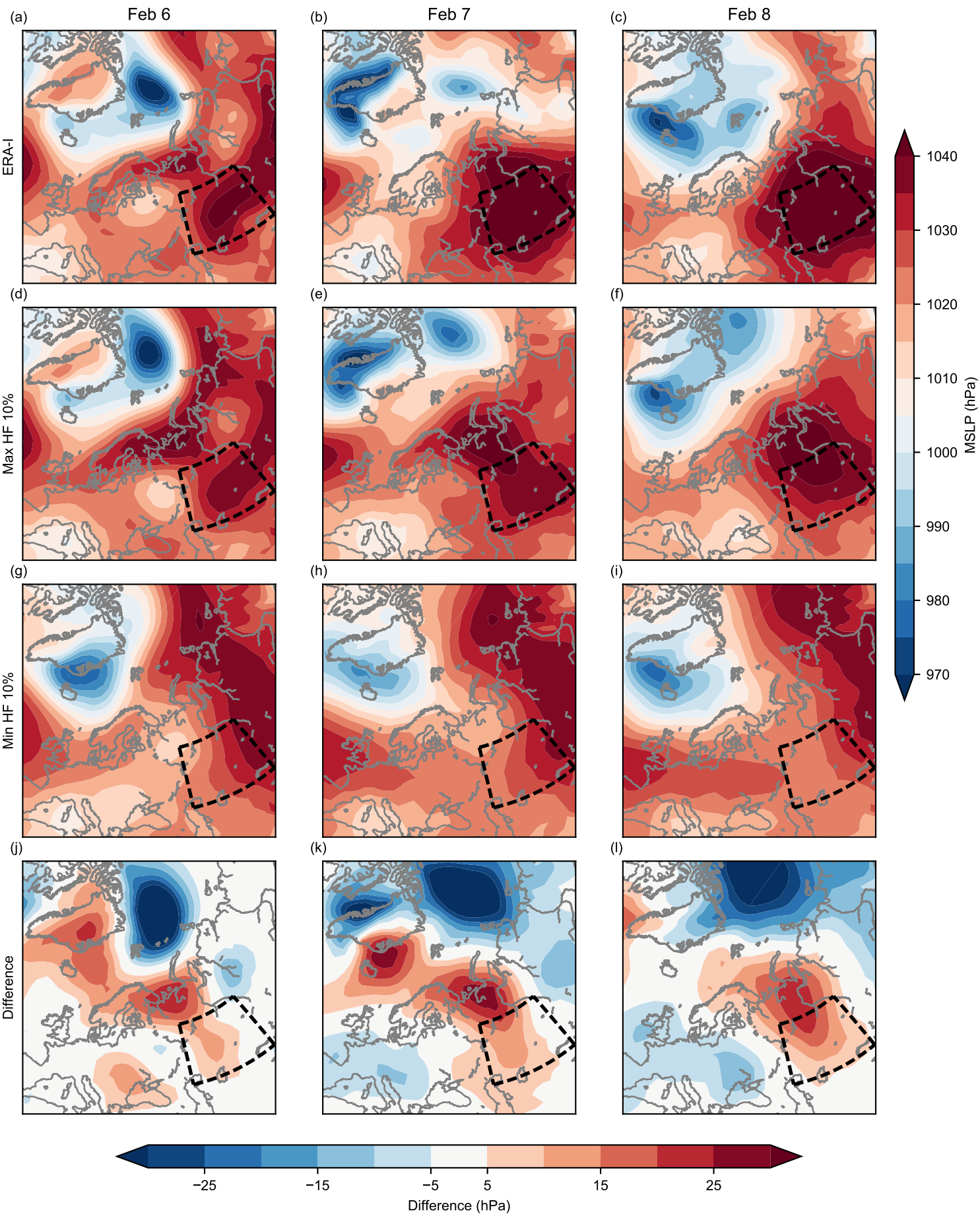
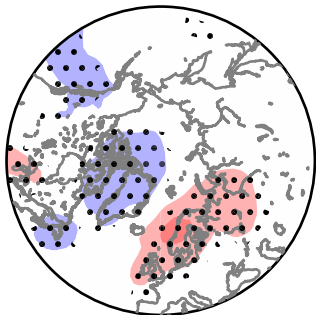
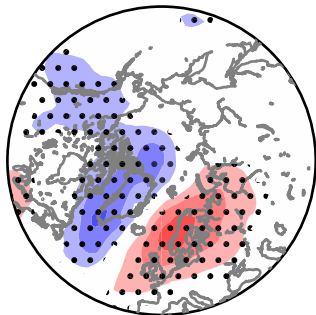


Figure 9.

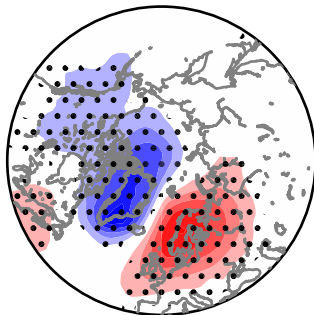
D-3



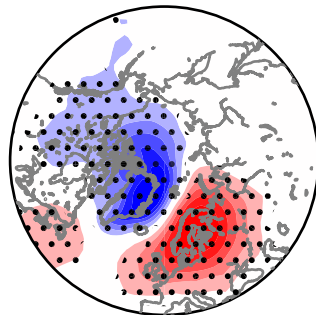
D-2



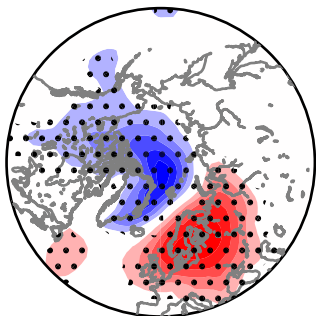
D-1



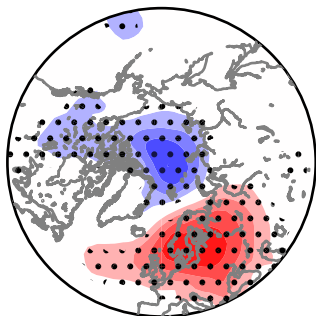
D0



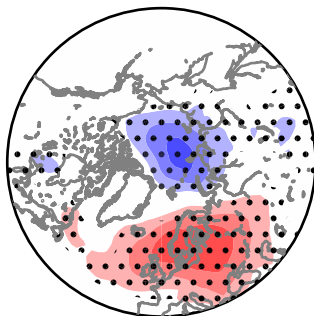
D1



D2



D3



D4

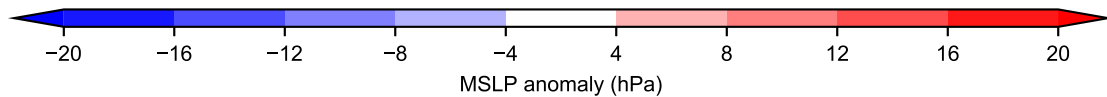
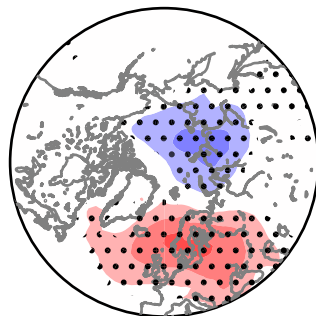
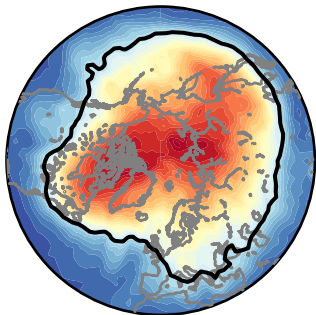
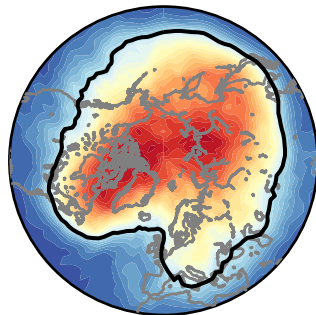


Figure 10.

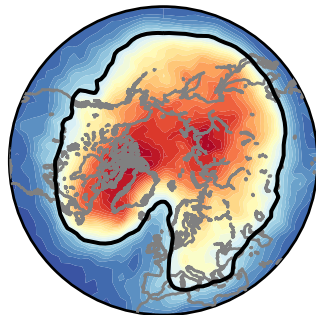
D-3



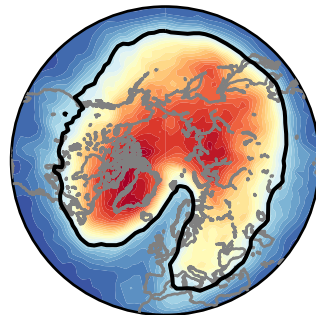
D-2



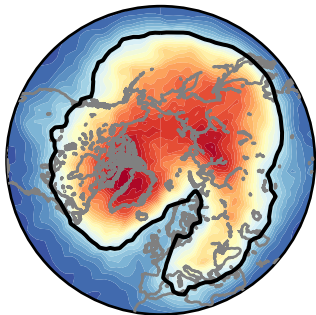
D-1



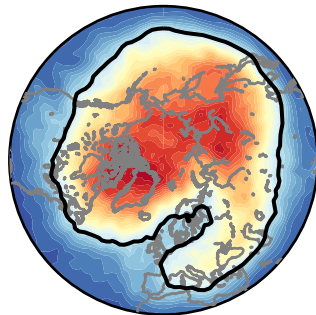
D0



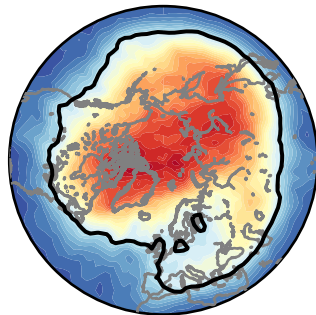
D1



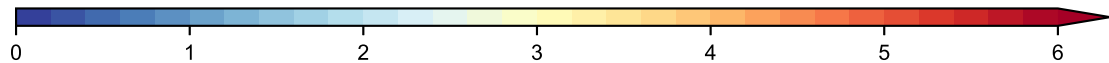
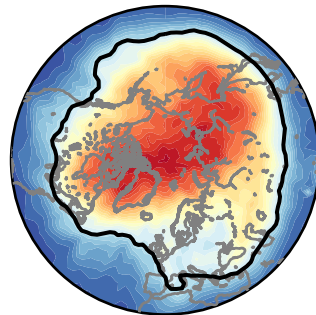
D2



D3



D4



0

1

2

3

4

5

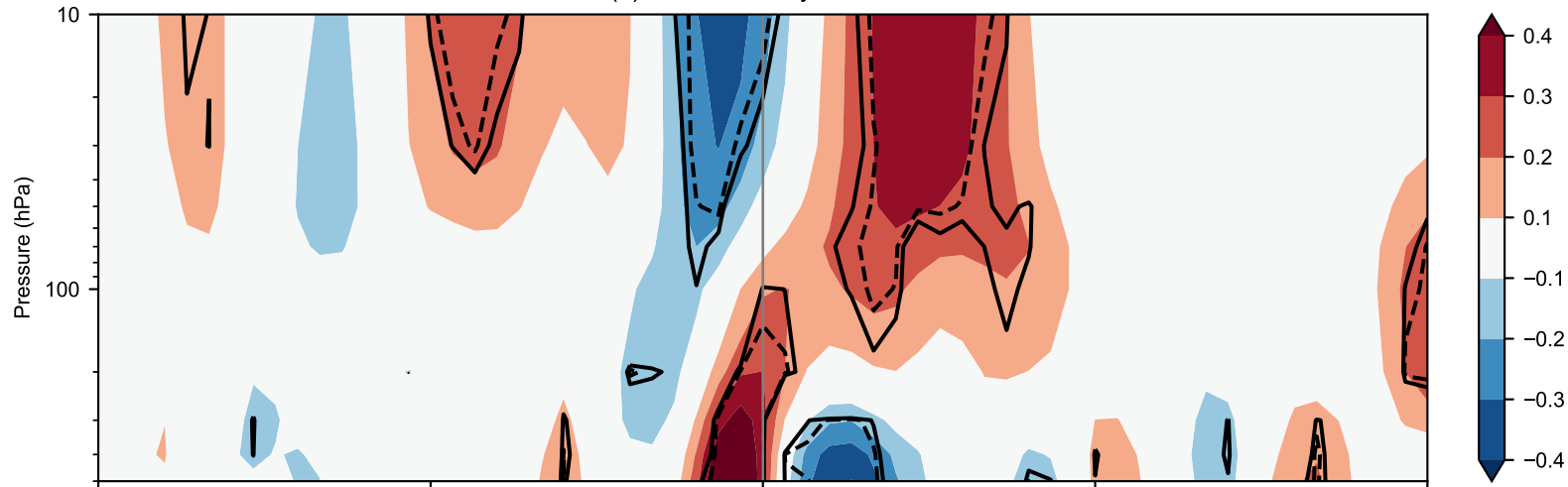
6

Potential Vorticity (PVU)

Figure 11.



(a) 45-75° N eddy heat flux



(b) 60-90° N geopotential height

